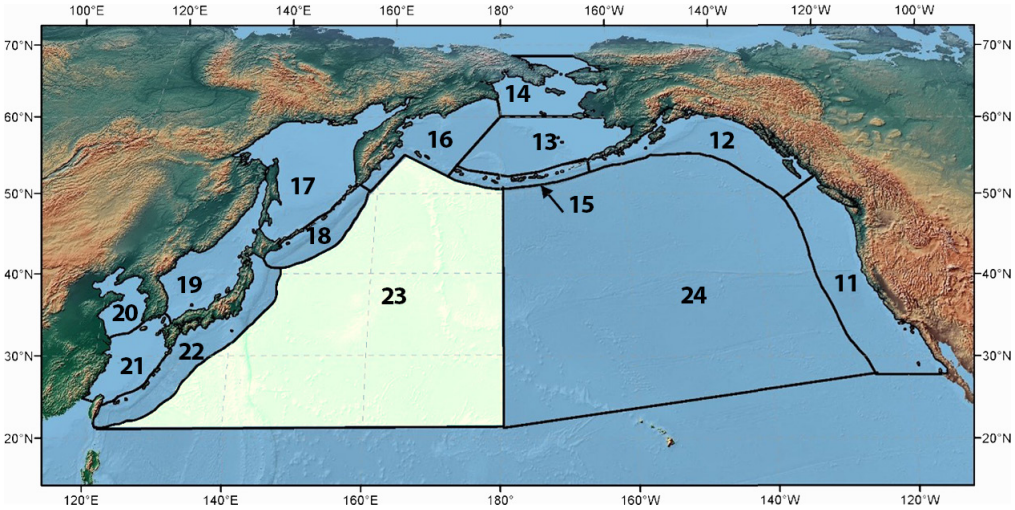

PICES

Regional Report for PICES Region:

23

PICES SPECIAL PUBLICATION 7

Marine Ecosystems of the North Pacific Ocean 2009–2016

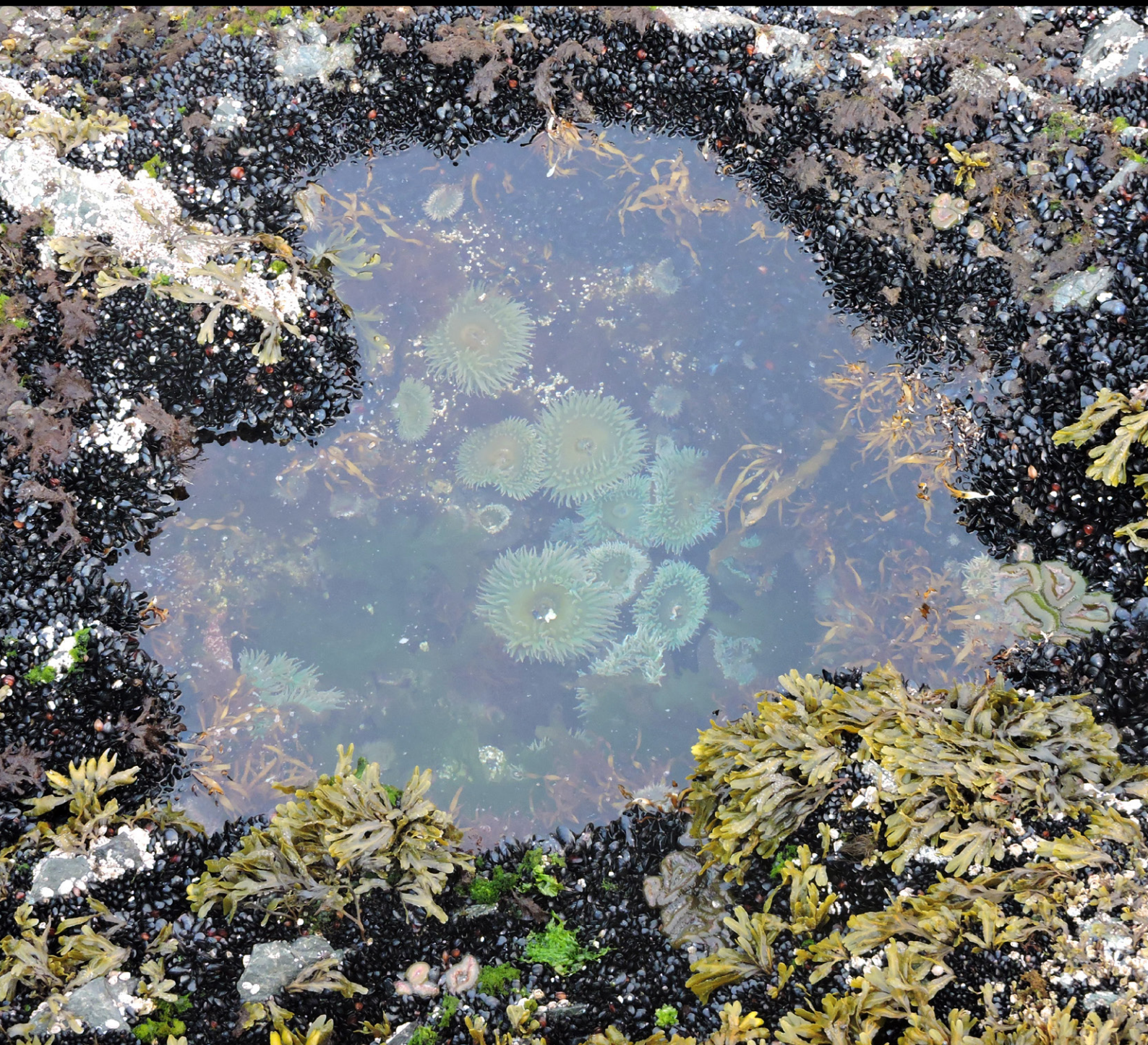

PICES North Pacific Ecosystem Status Report, Region 23 (Western Subarctic Gyre)

Tsuneo Ono: Fisheries Research Agency

Yokohama, Japan

Contributors:

Yu Kanaji[1], Hideki Kaeriyama[1], Naoki Nagai[2], Akira Nagano[3], Syu Saito[2], Eko Siswanto[3], Tsutomu Tamura[4], Sayaka Yasunaka[3], Tomoko M. Yoshiki[3], Masahide Wakita[3], Shiroh Yonezaki[1]

[1]Japan Fisheries Research and Education Agency

[2]Japan Meteorological Agency

[3]Japan Agency for Marine Science and Technology

[4]The Institute of Cetacean Research

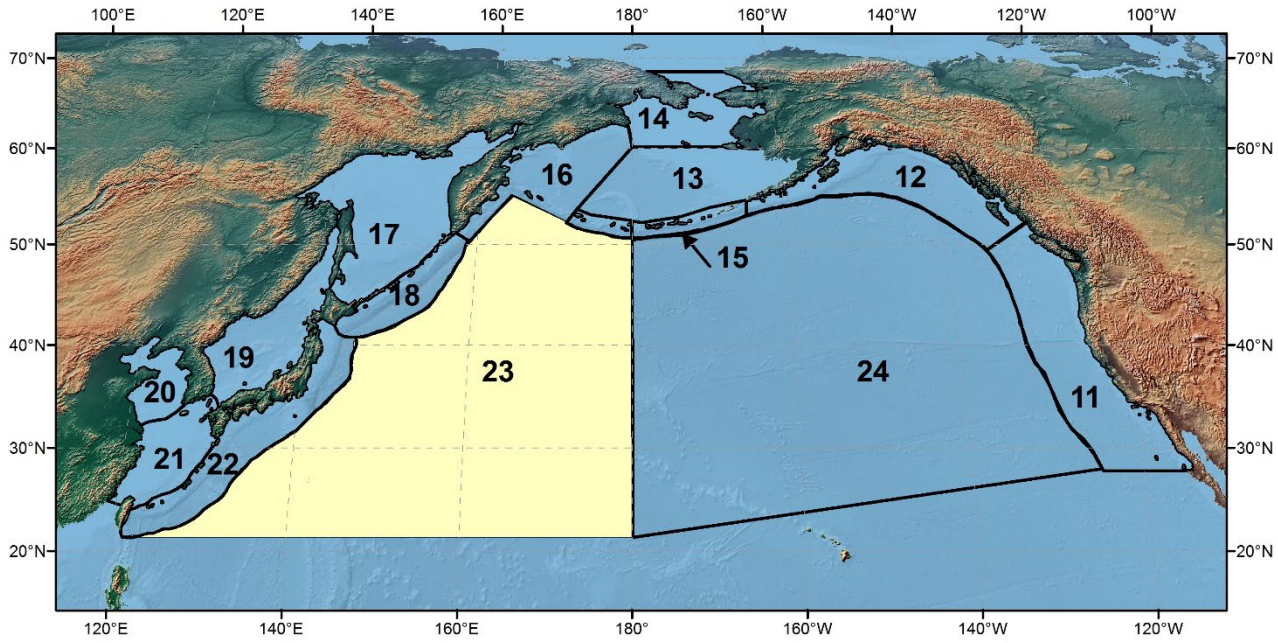

Figure R23-1. The PICES biogeographical regions and naming convention for the North Pacific Ocean with the area discussed in this report highlighted.

1. Highlights

- The Western Subarctic Gyre shrank northward during 1994 to 2008, and as a result, the mixed layer depth increased north of 47°N while it decreased south of that.
- The concentration of Chl-*a* increased north of 47°N while it decreased south of that.
- The habitat of warm-water copepod species shifted northward after 2007.
- Prey composition of sei whales appeared to reflect species composition changes of pelagic fishes in the Western Subarctic Gyre.

2. Introduction

The Western Subarctic Gyre (WSAG) has the most productive surface area in the open North Pacific. Annual net community production in the surface mixed layer in this area is about 4.1 molC/m^2/y (Palevsky et al., 2015), a value that is twice as large as it is in the eastern subarctic North Pacific (2.1 molC/m^2/y, Palevsky et al., 2015). This high productivity supports a high abundance of zooplankton (1950–4980 mg/m^2 in dry weight at the top 150 m; Steinberg et al., 2008), marking this area as the feeding migration area of commercially important fishes such as salmon, Pacific saury and Japanese pilchard. Whales and sea birds also use this area for feeding.

The WSAG adjoins with the Oyashio on its western boundary, and biogeochemical and ecological conditions of these two regions resemble each other. The most significant difference between these areas, however, exists in the limiting factors of phytoplankton in the summer season. While the phytoplankton community in the Oyashio area is dominated by diatoms and is limited by iron in spring, the community changes to a nanoplankton-dominated one in summer and the limiting factor changes to nitrate (Saito et al., 2002). In the WSAG, however, the phytoplankton community is dominated by diatoms throughout all seasons, and they are limited by the availability of light (Matsumoto et al., 2014) and iron (Tsuda et al., 2003). This results in a large difference in annual nutrient dynamics between the Oyashio and WSAG. While nitrate concentration in the summer mixed layer reaches close to zero in the Oyashio region, all major nutrients (N, P, and Si) remain to a certain extent in the summer mixed layer in the WSAG. This fact explains why net primary production (i.e., seasonal drawdown of the mixed layer nutrients) in the WSAG is still about half of that in the Oyashio region, despite similar nutrient levels in the winter mixed layer (Yasunaka et al., 2014a). This fact also indicates that the temporal variation of net community production in the WSAG is controlled both by the variation of winter nutrient loading and by variation of limitation factors (i.e. availability of light and iron) in summer phytoplankton communities. We discuss the observed temporal variation of these controlling factors, as well as the consequent variation of several biogeochemical parameters and ecosystems in the WSAG in the following sections.

Climate is essentially a large-scale phenomenon, and hence the WSAG experiences a similar climate variation with that of the Oyashio region. We, therefore, share the description of climate variation in the WSAG with that of the Oyashio (R18). We also share the information of pelagic fishes, as most of the commercial pelagic fishes living in the WSAG share their habitats with the Oyashio region. We acknowledge the readers for referring to the sections in R18 for these topics.

3. Atmosphere

Please see R18.

4. Physical Ocean

(A. Nagano)

Heat and materials in the western subarctic North Pacific are considered to be redistributed, associated with changes in physical conditions such as sea surface currents. The redistributions are critical to the climate and ecosystems. In addition, changes in the depths of the winter mixed layer or dichothermal (temperature minimum) layer have impacts on the biogeochemical systems within the western subarctic region. Owing to the accumulation of hydrographic data at stations K2 (47°N, 160°E) and KNOT (44°N, 155°E) from the mid-1990s, the temporal variability of the winter mixed layer (WML) base and decreasing potential density in winter by warming and freshening were revealed by Wakita et al. (2010, 2013, 2017).

There is a cyclonic circulation, called the western subarctic gyre (WSAG), in the western subarctic region (e.g., Dodimead et al., 1963; Favorite et al., 1976). The gyre is one of the subcirculations submerged within the subpolar gyre of the North Pacific. The western boundary current of the WSAG is called the East Kamchatka Current, which is fed to the Oyashio east of the Kuril Islands and Hokkaido. Through the geostrophic balance, the depth of the main pycnocline shoals toward the center of the WSAG. The gyre change is accompanied by the altimetric sea surface height (SSH) and the pycnocline (halocline) changes, and may be responsible for the WML depth in the western subarctic region. Nagano et al. (2016) found a decadal northward shrinkage of the WSAG from the later 1990s to the mid-2000s, accompanied by SSH elevation (Figure R23-2) and the associated deepening of the main pycnocline or halocline at K2. They also suggested that the pycnocline deepening is related to that of the dichothermal layer. The slow acidification in the western subarctic region (Section 5.2) was considered to be attributed to the reduced rate of increase of dissolved inorganic carbon caused by the pycnocline depression, the weakened vertical mixing flux and warming, and the increase of total alkalinity (Wakita et al., 2017).

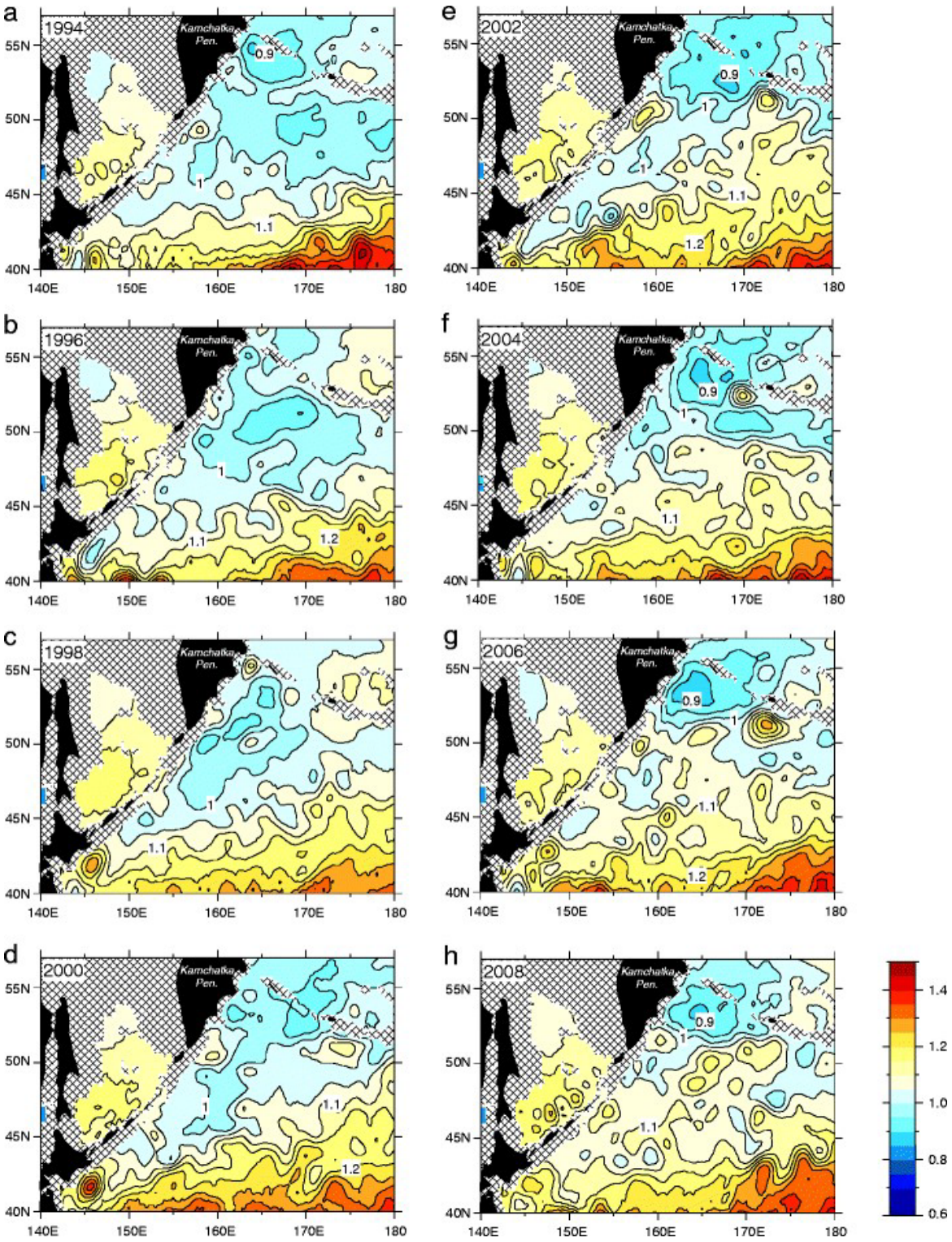

Figure R23-2. Decadal change of altimetric sea surface height (SSH) in the western subarctic region of the North Pacific from (a) 1994 to (h) 2008. Contour interval is 0.05 m. Mesh indicates no data. After Nagano et al. (2016).

5. Chemical Ocean

5.1. Nutrients

(S. Yasunaka)

The National Institute for Environmental Studies (NIES, Japan) and the Institute of Ocean Sciences (IOS, Canada) have carried out ship-of-opportunity measurements of nutrients (phosphate, nitrate, and silicate) and partial pressure of CO_2 since the late 1980s (Whitney 2011; Nakaoka et al., 2013; Yasunaka et al., 2014a). Using the ship-of-opportunity and other data sets, long-term variability of sea surface nutrients in the North Pacific were clarified. The Pacific Decadal Oscillation was related to a nutrient seesaw pattern between the subarctic–subtropical boundary region and the Alaskan Gyre through changes in horizontal advection, vertical mixing and biological production (left panels in Figure R23-3; Yasunaka et al., 2013, 2014b, 2016). When the North Pacific Gyre Oscillation was in the positive phase, nutrient concentrations in the subarctic were higher than the mean states (right panels in Figure R23-3; Yasunaka et al., 2016). Trends of phosphate and silicate averaged over the North Pacific were negative, while the nitrate trend was insignificant (Figure R23-4).

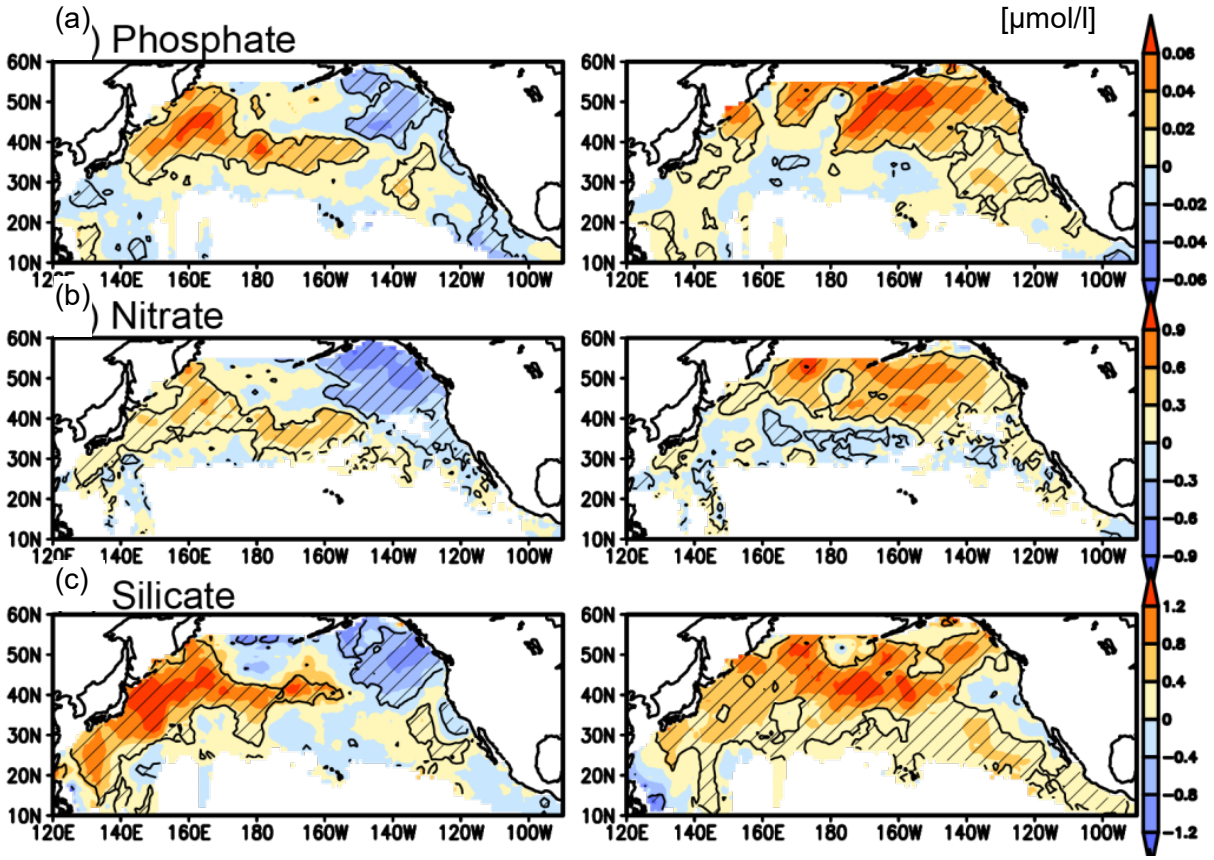

Figure R23-3. (a) Phosphate, (b) nitrate, and (c) silicate regression patterns onto the Pacific Decadal Oscillation (PDO) index (left panels), and the North Pacific Gyre Oscillation (NPGO) index (right panels). Shaded areas indicate regression coefficients significant at $p < 0.05$. After Yasunaka et al. (2016).

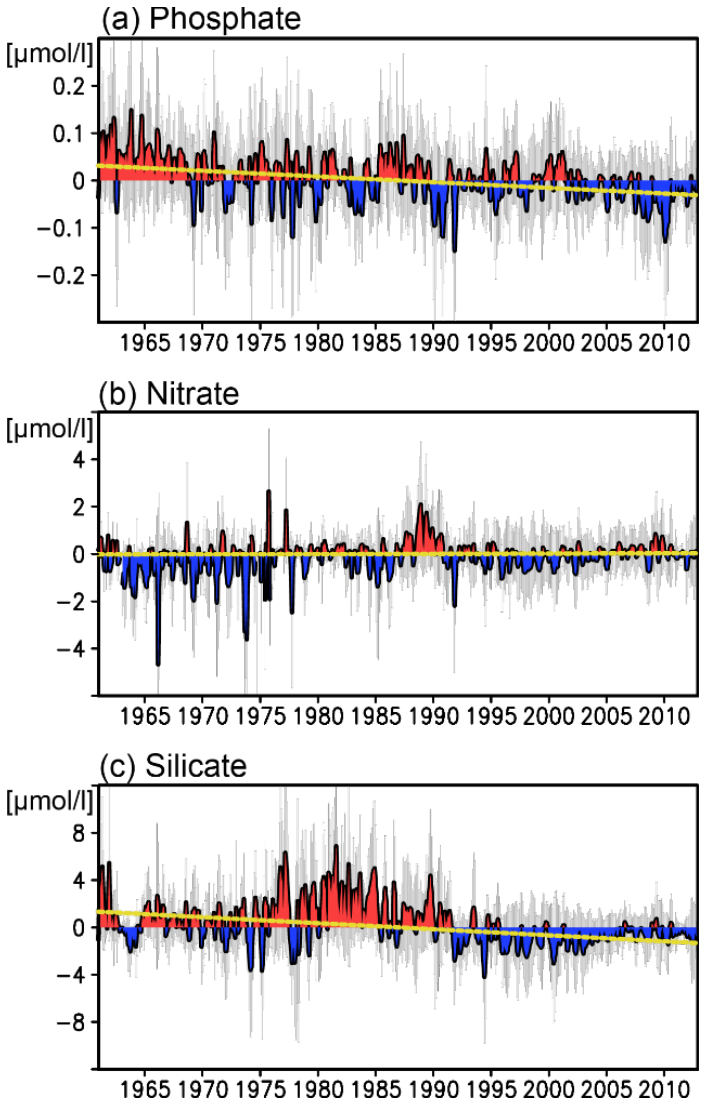

Figure R23-4. (a) Phosphate, (b) nitrate, and (c) silicate concentration anomalies after subtracting the PDO- and NPGO-related variabilities averaged over the North Pacific (red and blue shadings). Gray error bars denote standard deviations of the averages. Yellow line denotes regression coefficient of the trend time series averaged over the North Pacific. After Yasunaka et al. (2016).

5.2. CO_2 and pH

(M. Wakita)

Approximately 30% of the total amount of carbon dioxide (CO_2) released into the atmosphere by human activities (i.e., anthropogenic CO_2) has accumulated in the global ocean (IPCC, 2013). This oceanic uptake of anthropogenic CO_2 has resulted in the acidification of sea surface waters, the observed decrease of pH being 0.1 since the beginning of the industrial era (IPCC, 2013). Ocean acidification increases the hydrogen ion (H^+) concentration (i.e., lowers the pH) and lowers the $CaCO_3$ saturation state (Ω) by decreasing the carbonate ion (CO_3^{2-}) concentration with a concomitant formation of bicarbonate ions (HCO_3^-). These carbonate chemistry changes may be affecting marine organisms and ecosystems throughout the global ocean (e.g., Doney et al., 2009).

The subarctic western North Pacific is characterized by high primary productivity and abundant marine resources (FAO, 2016). Ocean CO_2 time-series sites have been established at 47°N, 160°E (K2) and at 44°N, 155°E (KNOT) in the western subarctic gyre (e.g., Tsurushima et al., 2002; Wakita et al., 2013, 2016, 2017). The difference in pCO_2 between sea surface water and atmosphere at these sites have seasonal cycles. From spring to fall, the western subarctic region is a sink for CO_2 due to biological production. In winter, it is a source of CO_2 to the atmosphere due to strong vertical mixing of deep waters rich in dissolved inorganic carbon (DIC).

Ocean acidification in the surface water at station K2 has progressed as a result of oceanic uptake of anthropogenic CO_2 from the atmosphere (Wakita et al., 2017). Annual mean pH (total scale) at the in-situ temperature ($pH_T^{in\ situ}$) at K2 decreased significantly during 1999–2015 at rates of 0.0025 ± 0.0010 yr^{-1} (Figure R23-5, left panel). The rate of increase of oceanic pCO_2 was similar to that of atmospheric pCO_2 (Figure R23-5, right panel). The trends of these parameters were similar to the analogous trends at other sites, including the BATS, HOT, ESTOC, CARIACO, Irminger Sea, and Munida Time Series sites noted by Bates et al. (2014). However, the rate of increase of the annual mean Revelle factor (0.046 ± 0.022 yr^{-1}) was higher than the corresponding rates (0.011–0.030 yr^{-1}) at the sites noted by Bates et al. (2014). This difference indicates that the capacity of the western subarctic region to absorb CO_2 from the atmosphere is lower than that of the other sites and has been reduced over time faster than at the other open time-series ocean sites. Marine organisms, especially calcifying species, and ecosystems might be very susceptible to acidification in this region.

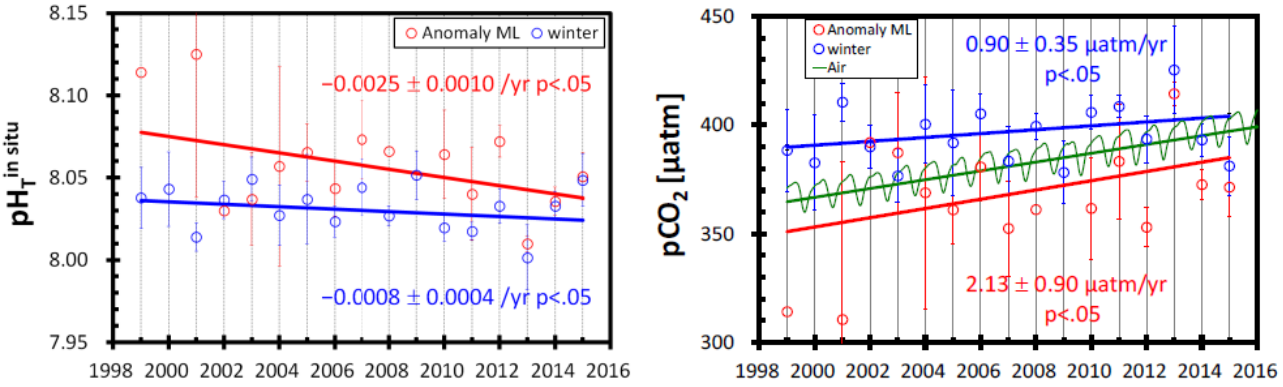

Figure R23-5. Time-series of $pH_T^{in\ situ}$ (left panel) and oceanic and atmospheric pCO_2 (right panel) in the western subarctic region. The circles and vertical lines are annual means and standard deviations in the surface mixed layer at K2 (red circles) and in the winter mixed layer at K2 and KNOT (blue circles). The light green curve shows the atmospheric pCO_2 calculated from the zonal average time-series at 48.6°N of the volumetric mixing ratio of CO_2 in dry air from 1999 to 2015 (NOAA Greenhouse Gas Marine Boundary Layer Reference; Dlugokency et al., 2014) and the saturation vapor pressure of water (Weiss and Price, 1980) at the annual mean sea surface temperature (SST) and sea surface salinity (SSS) at K2 in an assumed water-saturated interface. The regression lines (solid lines) indicate significant trends ($p < 0.05$). The error values are the standard error of the slope of the liner regressions. After Wakita et al. (2017).

In addition, as the anthropogenic CO_2 accumulated in the ocean interior, the $CaCO_3$ saturation horizon below the dissolution of $CaCO_3$ occurs, shoaled as a function of the decrease in Ω (e.g., IPCC, 2013). The $CaCO_3$ saturation horizon with respect to the two mineral forms of $CaCO_3$, aragonite and calcite, in the western subarctic region is the shallowest of any location in the open ocean, because [CO_3^{2-}] (and hence Ω) is low (Feely et al., 2004, Wakita et al., 2013). Wakita et al. (2013) reported a shoaling of the calcite

saturation horizon at 2.9 ± 0.9 m yr^{-1} from 1997 to 2011, and that shoaling continued until at least 2015. During the same time interval, the aragonite saturation horizon remained at a depth of approximately 120 m, below the bottom of the winter mixed layer. In the future, the western subarctic Pacific will be the first region of the ocean to become undersaturated with respect to $CaCO_3$ in the winter (Orr et al., 2005) because winter Ω is lower and is caused by the convective mixing of deep waters rich in DIC, accompanied by a strong CO_2 source (e.g.,Tsurushima et al., 2002; Wakita et al., 2013). Marine calcifying organisms with carbonate shells and skeletons (e.g., pteropods, coccolithophores, and foraminifera) in this region may be the first organisms to disappear from the open ocean as a result of ocean acidification.

The rate of acidification in winter was quite different from the annual mean rate (Wakita et al., 2013, 2017; Figure R23-5). The rate of $pH_T^{in\ situ}$ decline in winter (0.0008 ± 0.0004 yr^{-1}, $p < 0.05$) was slower than the annual mean rate, whereas the decreasing trends of Ω, $[CO_3^{2-}]$, and the Revelle factor in winter were insignificant despite those significant annual mean rates (Wakita et al., 2017). The slower winter acidification was caused by a reduction of the rate of increase of salinity-normalized DIC (nDIC) and an increase of salinity-normalized total alkalinity (nTA) (Wakita et al., 2017). The reduction of the rate of increase of the nDIC in winter is attributed to a reduction of the surface water density due to the pycnocline depression associated with the northward shrinkage of the western subarctic gyre (Nagano et al., 2016) and surface water warming, and a decline of the vertical diffusion flux of deep water with high concentrations of nDIC from the top of the main pycnocline as a result of the decreased vertical gradients of nDIC and the weakened stratification due to the northward gyre shrinkage. Because the nTA increase in winter due to the decrease in density is cancelled out by the reduction of the vertical diffusion flux, the increase of winter nTA is possibly caused by weakening calcification in organisms in winter.

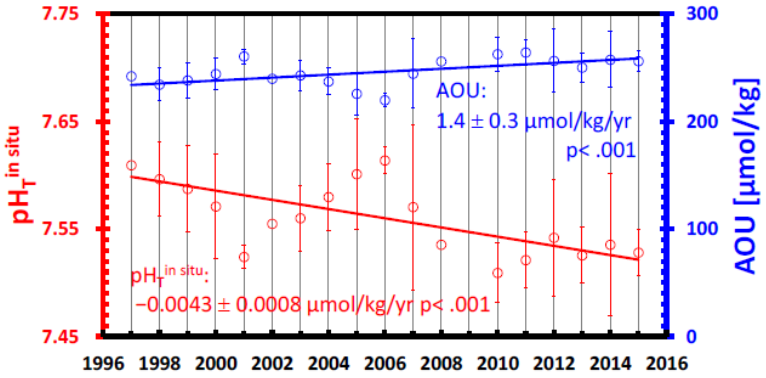

Figure R23-6. Time-series of $pH_T^{in\ situ}$ (red, left y axis) and the apparent oxygen utilization (AOU) (blue, right y axis) on the 26.9σ_θ surface in the western subarctic region. This figure updates the results from Wakita et al. (2013) by adding data from 2012–2015. The regression lines for $pH_T^{in\ situ}$ (red line) and AOU (blue line) indicate significant trends ($p < 0.001$). The error values are the standard error of the slope of the linear regressions.

Below the surface mixed layer, the rate of $pH_T^{in\ situ}$ decline during 1997–2015 at about 200 m depth (0.0043 ± 0.0008 yr^{-1}, $p < 0.001$) (Figure R23-6) was larger than ever reported for the open North Pacific (e.g., Dore et al., 2009; Byrne et al., 2010). The enhanced pH decline reflected not only uptake of anthropogenic CO_2 but also the increase in the remineralization of organic matter evaluated from the increase in apparent oxygen utilization (Figure R23-6), which suggests that the dissolution of sinking $CaCO_3$ particles increased (Wakita et al., 2013).

6. Phytoplankton

(E. Siswanto)

Based on merged SeaWiFS and MODIS-derived phytoplankton biomass (CHL, mg m^{-3}) within the period from 1997 to 2013, the recent trend of CHL in the western North Pacific subarctic region (SAR) was investigated. Over high latitudes of about 47°N, CHL within the last 16 years has tended to increase significantly (Figure R23-7a). Combined AVHRR and MODIS-derived sea surface temperature (SST, °C) in the SAR has tended to increase significantly, except south of 42°N and west of 160°E (FigureR23-7b).

Increased SST may reduce vertical nutrient input (by strengthening water column stratification), and thus can be detrimental for phytoplankton. However, rather than being affected by reduced nutrients, phytoplankton north of 47°N likely benefit more from increased SST, as this promotes phytoplankton growth. This is supported by Fujiki et al. (2014) and Matsumoto et al. (2014) who suggested that, rather than being limited by nutrients, phytoplankton in the SAR are more limited by temperature and/or light.

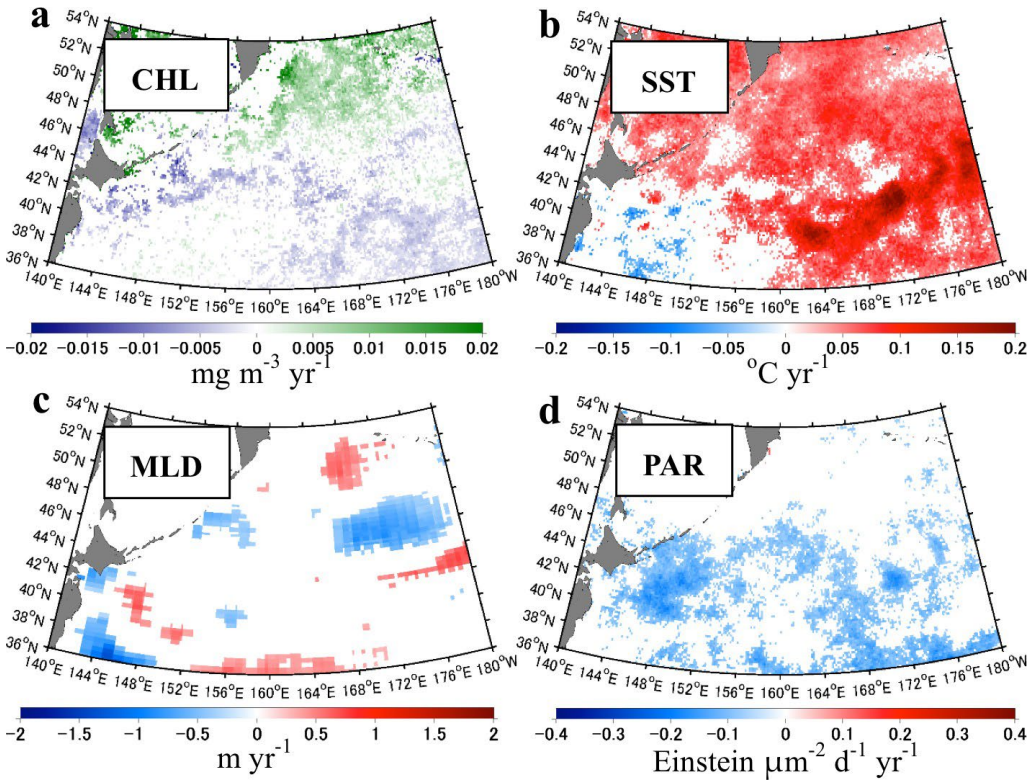

Figure R23-7. Spatial variations of 16-year (1997–2013) trends of (a) CHL, (b) SST, (c) MLD, and (d) PAR in the SAR. White color indicates the area where trend is statistically insignificant (by Mann-Kendall test with 95% confidence level). Prior to trend analysis, the seasonal cycle of variables was removed by subtracting the monthly climatological mean from data time series (see Siswanto et al. (2016a) for detailed methodology).

Unclear and insignificant trends of mixed layer depth (MLD, m) (Figure R23-7c) and photosynthetically available radiation (PAR, Einstein $\mu m^{-2} d^{-1}$) (Figure R23-7d) also indicate that light might not be responsible for the increasing trend of CHL. In addition, partial regression

coefficients (β) resulting from multiple linear regression which are positive for PAR (βPAR, R23-8c), negative for MLD (βMLD, Figure R23-8b), and positive for SST (βSST, Figure R23-8a), particularly north of 47°N, also support that the increasing trend of CHL north of 47°N is indeed likely attributable to increasing SST.

A large portion of the region south of about 47°N shows a significant declining trend of CHL (except for the area south of 42°N and west of 160°E), indicating that phytoplankton south of 47°N are more likely to experience a detrimental effect of increasing SST (by reducing vertical nutrient input) than a beneficial effect (by promoting phytoplankton growth). A less significant increasing trend of CHL was, however, observed over the area south of about 42°N and west of 160°E. Such a trend is likely attributed to a tendency for elevated nutrient input from the deep layer as indicated by a tendency of declining SST over the same area (Figure R23-8b). This is supported by the fact that phytoplankton there are more limited by nutrients than by temperature and/or light as indicated by negative βSST (Figure R23-8a), which is more significant than negative βMLD (Figure R23-8b).

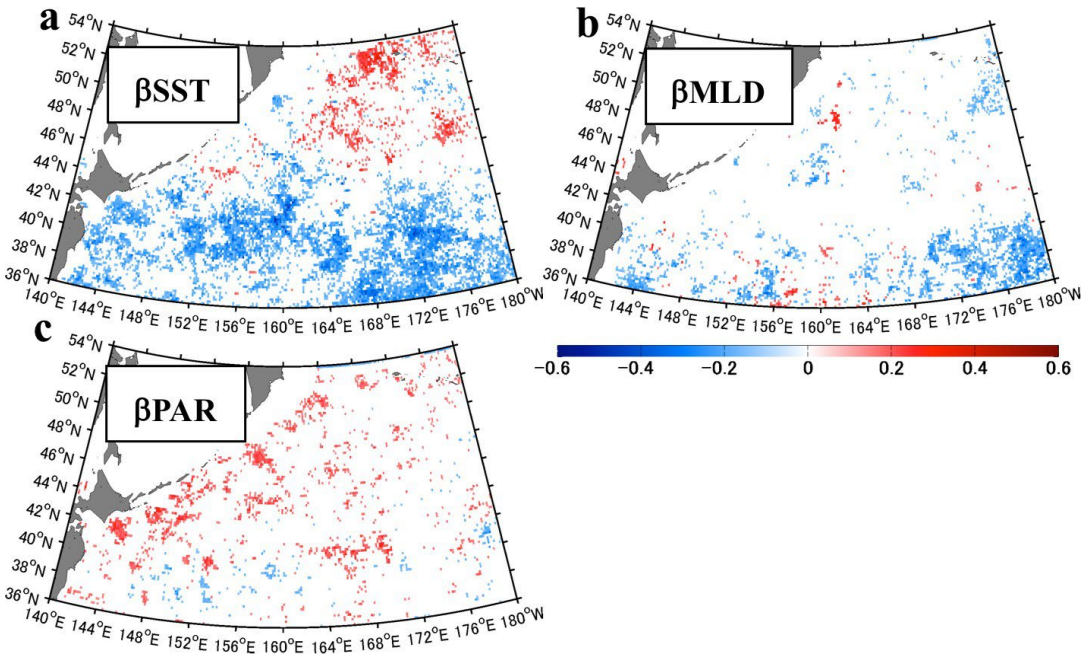

Figure R23-8. Spatial variations of (a) βSST, (b) βMLD, and (c) βPAR derived from a multiple linear regression [CHL= f(SST, MLD, PAR)]. All variables were standardized with Z-score transformation (e.g., Nathans et al., 2012). White color indicates the area where β is statistically insignificant at a 95% confidence level (see Siswanto et al. (2016a) for detailed methodology).

Using the same datasets, a detailed spatial response of phytoplankton in the SAR to El Niño climate variability was investigated. An El Niño footprint was inferred from the correlation coefficient (r) derived by linear regression of variables (e.g., CHL) on Niño3.4, where a positive (negative) phase indicates El Niño (La Niña). An intense Aleutian Low pressure system during an El Niño event leads to strengthened westerly winds, as depicted by a deepened MLD over almost the entire SAR (i.e., positive r in Figure R23-9c). A deepened MLD is likely effective to entrain cold (hence nutrient-rich) deep water over the area south of 47°N (Figure R23-9b, see SST – Niño3.4 negative r). SST north of 47°N, on the other hand, tends to increase during El Niño. The response of PAR to El Niño is less obvious than to other variables (Figure R23-9d).

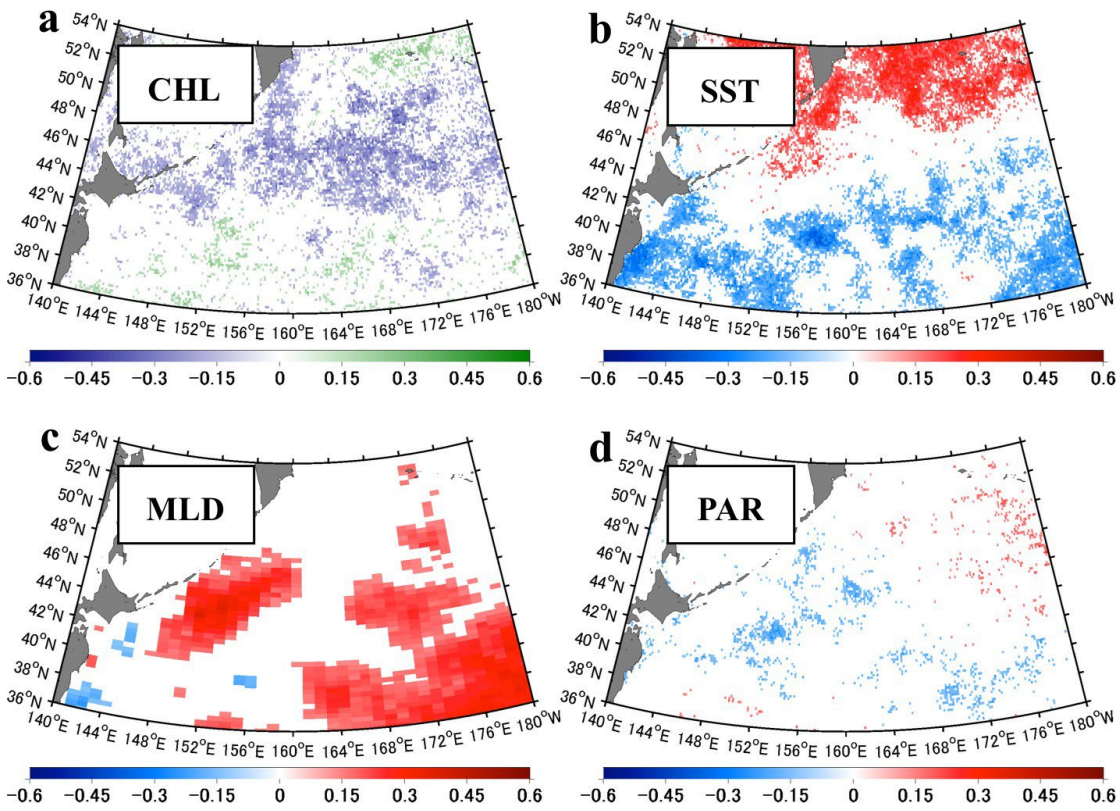

Figure R23-9. Spatial variation of r resulting from the regression of (a) CHL, (b) SST, (c) MLD, and (d) PAR on Niño3.4. The area with insignificant r at a 95% confidence level is masked out (white areas). Prior to regression, the monthly climatological mean and long-term trend were removed from time series data (see Siswanto et al. (2016b) for detailed methodology).

Phytoplankton exhibited a meridionally different response to a deepened MLD (Figure R23-9a), i.e., south of 42°N, and CHL tended to increase (positive r); between 42°N and 51°N, CHL tended to decline (negative r); and to the north of 51°N CHL tended to increase (positive r). Increasing CHL south of 42°N during El Niño was likely attributed to increased nutrients due to a deepened MLD. This is understandable because phytoplankton south of 42°N are limited more by nutrients than by light as indicated by a more pronounced negative βSST (Figure R23-8a) than negative βMLD (Figure R23-8b) and positive βPAR (Figure R23-8c).

Phytoplankton north of 42°N are also likely limited by light, as indicated by a negative βMLD and positive βPAR. Therefore, declining CHL over the area between 42°N and 51°N during an El Niño event likely indicates that phytoplankton in this area are more sensitive to a reduction of mean light within the MLD (due to a deepened MLD) rather than to an increase in nutrients (also due to a deepened MLD). Further northward of 51°N, however, CHL again tended to increase. This may indicate that phytoplankton over this area are more sensitive to increasing SST (Figure R23-9b) than reduced light within the MLD. In other words, phytoplankton growth rate (promoted by increased SST) might still be higher than phytoplankton loss rate (caused by declining light due to a deepened MLD) resulting in a positive net growth and manifested by an increase in CHL.

7. Zooplankton

(T. M. Yoshiki)

Spatial and temporal variation in copepod community structure, abundance, latitudinal distribution, developmental stage of large sized cold-water species and biodiversity were examined in the western subarctic North Pacific (40–53°N, 144–173°E) by using Continuous Plankton Recorder (CPR) observational data during the summer season (June and July) from 2001–2013 (Yoshiki et al., 2015). Copepod species were classified into three groups: cold-water species, warm-water species and other species, according to the descriptions of Chihara and Murano (1997). The most abundant species in each group were *Neocalanus plumchrus* for cold-water species, *Calanus pacificus* for warm-water species and *Oithona similis* for other species. Cold-water species and other species occurred in all sampling areas, and no significant correlation was observed between these abundances and sea surface temperature (SST). Comparing the latitudinal distributions of copepod species groups, no notable variation in the latitudinal distribution of both cold-water and other species groups was observed. On the other hand, a small number of warm-water species occurred only in the southern area (<45°N) in the summer season during 2001–2007, and the latitudinal distribution of warm-water species groups shifted to the northern area at 52°N after 2008 (Figure R23-10). The abundance of warm-water species also increased after 2009, and a highly positive significant correlation was observed between SST and the abundance of warm-water species at each sampling location (0.628, $P < 0.0001$). In addition, the center of the latitudinal distribution of warm-water species was significantly correlated with SST ($r = 0.772$, $P < 0.005$), whereas no distinguished variations in the latitudinal distribution of cold-water and other species were observed.

Although there was no obvious variation in the latitudinal distribution of cold-water species, yearly variations were observed in the average developmental stage of the most abundant cold-water species: *Eucalanus bungii*, *Neocalanus plumchrus* and *N. flemingeri*. The average stage of *E. bungii* in June was comparatively younger during 2001–2003, and more mature during 2004–2011, and again younger in 2012 (Yoshiki et al., 2013, 2015). The average developmental stage of both *N. plumchrus* and *N. flemingeri* in June was more mature in 2011 and 2012 than that in 2001–2007. Studies on the effect of temperature on the developmental timing of these abundant cold-water species have indicated that developmental timing in species of *Neocalanus* is only minimally affected by the sea surface environment (Kobari and Ikeda, 2001; Tsuda et al., 2004; Yoshiki et al., 2013), whereas the developmental timing of *E. bungii* is subject to both SST and phytoplankton conditions (Tsuda et al., 2004; Kobari et al., 2007; Takahashi and Ide, 2011; Yoshiki et al., 2013). In contrast, several previous reports from the eastern North Pacific have demonstrated that warmer water temperatures promote growth and increase survival rates of *Neocalanus* species (e.g., Bornhold et al., 1998; Batten et al., 2003). Together, these observations suggest that increasing SST does not necessarily negatively affect all ‘cold-water’ species, especially species of *Neocalanus*. Rather, warmer temperatures might favor conditions amenable to the survival of some cold-water species.

Species number and the Shannon–Wiener biodiversity index (H') in June tended to increase in the northern area after 2011. Warm SSTs after 2011 appeared to cause the northward shift of warm-water species distribution, which contributed to the higher biodiversity in the northern area. This study demonstrated the rapid response of warm-water species to warm SST variation, whereas cold-water and other species did not exhibit such clear responses. These findings indicate that the response of copepods to environmental changes differs among copepod species, highlighting the importance of investigating lower trophic levels to the species level in order to evaluate individual species’ responses to climate change.

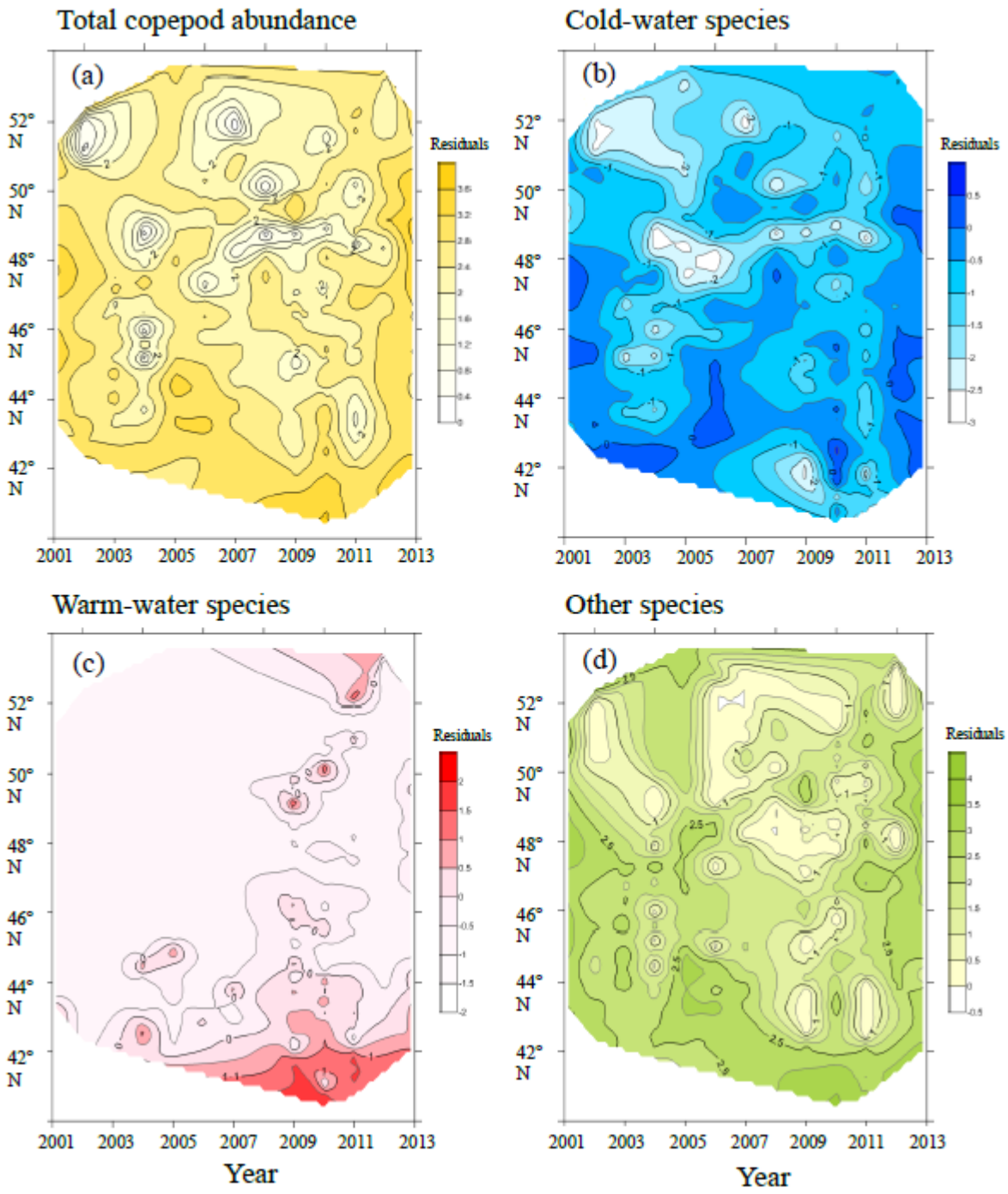

Figure R23-10. Latitudinal and interannual variation in copepod abundance using a residuals method to correct the biases of sampling Julian date, day/night, and longitudinal sampling locations. (a) Total copepod abundance, (b) cold-water species, (c) warm-water species, and (d) otherspecies. The cold-water species and other species occurred at almost all latitudes throughout the sampling period (b, d). By contrast, a few warm-water species occurred only in areas south of 46°N during 2001–2005, and a northerly shift in this group to the area north of 47°N after 2008 was detected (c).

8. Fishes and Invertebrates

8.1. Pelagic fishes

Please see R18.

8.2. Ground fishes

(S. Yonezaki)

The Emperor Seamount chain (ES) spans from 30°N to 55°N and from 168°E to 178°E, extending from the northwestern Hawaiian Islands to the Aleutian Trench in the western North Pacific, and is one of such seamount chains in the western North Pacific Ocean. In particular, the southern ES region is a bottom fisheries ground, targeting demersal fishes such as North Pacific armorhead (*Pentaceros wheeleri*; NPA) and splendid alfonsino (*Beryx splendens*).

Bottom fisheries in the southern ES region were developed by the trawl fleet of the former Soviet Union in 1967. The Japanese fleet joined the trawl fishery in 1969. The Korean commercial trawl fleet started fishing in the region in 2004. Japanese trawl and gill net vessels and Korean trawl vessels have been operating in the region, although Russian vessels have not conducted NPA fisheries since 2007. The history of NPA fisheries starts with a short period of large catch, followed by a rapid decrease and a long period of low catch levels with several episodic increases (FigureR23-11). During the initial phase of exploitation in the region, the annual total catch of this species surpassed 100,000 metric t in 1969, 1970, 1972, and 1973. The commercial catch declined rapidly in 1977 and thereafter remained at very low levels (< 2,000 metric t in most years). However, sudden increases of the catch were recorded several times, e.g., in 1992, 2004, 2005, 2008, 2010 and 2012, reflecting strong recruitment. Especially in 2010 and 2012, total annual catches were above 20,000 metric t and were the largest after 1976. However, the catch levels have remained low for five consecutive years since 2013.

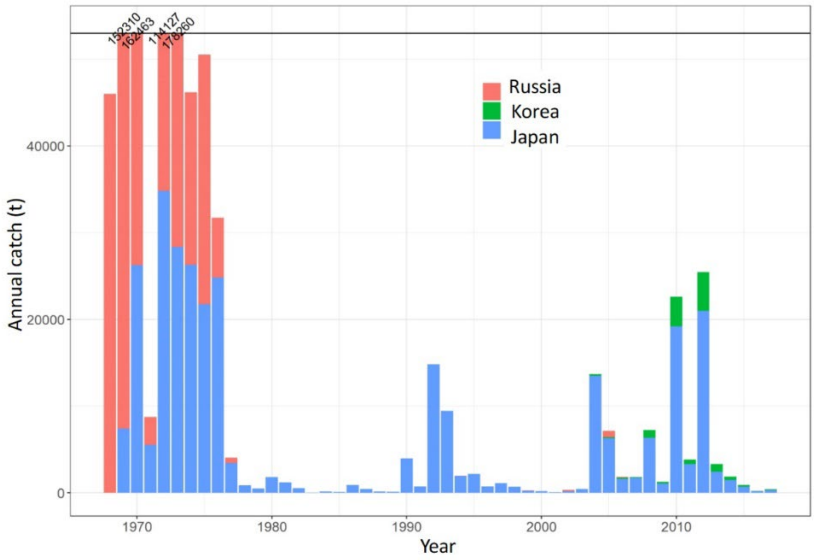

Figure R23-11. Historical trends in annual commercial catches (in metric tons, t) of North Pacific armorhead (*Pentaceros wheeleri*) in the southern ES region by the former Soviet Union (USSR) and Russia, Japan, and Korea. Modified from Fisheries Agency of Japan and Japan Fisheries Research and Education Agency (2019), http://kokushi.fra.go.jp/H30/H30_74.pdf.

NPA have a unique life history with a long epipelagic period, determinate growth and weight loss (Kiyota et al., 2016). Larvae are found in the surface waters around the southern ES region whereas juveniles and subadults migrate to and grow in the epipelagic layer of subarctic Northeast Pacific Ocean for 2.5 to 4 years (epipelagic life stage) (Murakami et al., 2016). After they have attained maturation size (≥ 25 cm in fork length), subadults settle to the seamount summit and shift to the demersal life stage in spring or summer. After settlement, they start maturation and cease growth of body length (determinate growth). Those newly settled fish are called “fat type” because their bodies are deep (high) and fatty. Demersal individuals reproduce each winter (November to February) and gradually change body proportion to the “lean type” by consuming fat reserves and losing body depth and weight (Figure R23-12). Little is known about the diets of NPA for both life stages, but Nishida et al. (2016) found Thecosomata and Porifera from the stomachs of demersal individuals. Further studies on unique changes in body proportion, which may be related to the feeding habit, are underway. Although demersal stage individuals were also found from the western Pacific Ocean off Japan and west coast of North America, spawning has been confirmed only around the southern ES region (Boehlert and Sasaki, 1988).

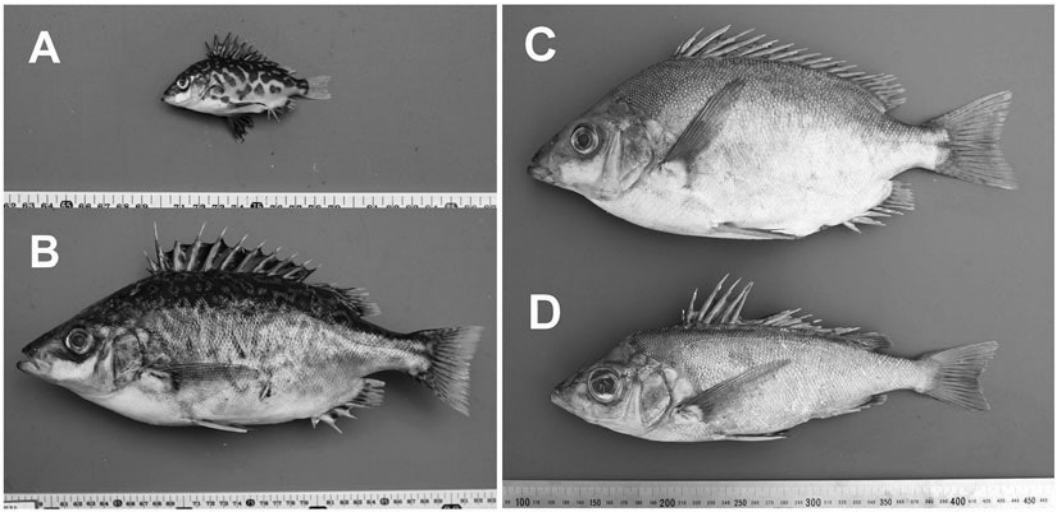

Figure R23-12. Photographs of North Pacific armorhead (NPA). (A) Pelagic juvenile, (B) pelagic subadult, (C) demersal adult (fat type), (D) demersal adult (lean type). From Kiyota et al. (2016).

The number of recruits (fish settled onto seamounts) varies greatly among years (Kiyota et al., 2016), and strong recruitment results in a strong increase in biomass because the recruits have already attained maximum body size. The fluctuation in recruitment is unpredictable and obscures the spawner–recruit relationship. In addition, since they do not grow (in length) at the fishing grounds, length-based age estimation and length-structured models are not applicable to this stock. However, “fatness” enables a rough distinction between newly recruited fish and older ones. Nevertheless, it is very difficult to conduct conventional stock assessment for fisheries management.

Since most of the ES region is located in the high seas, this fishing ground is managed under an international framework. Intergovernmental meetings were held in 2006 to establish a new regional fishery management organization in the North Pacific region to ensure the long-term conservation and sustainable use of the fisheries resources (including North Pacific armorhead), while protecting the marine ecosystems in which these resources occur. The *Convention on the Conservation and Management of High Seas Fisheries Resources of the North Pacific Ocean* was adopted in February 2012, and came into force in July 2015. The convention established the North Pacific Fisheries Commission (NPFC) in September 2015 (Moon, 2017).

The NPFC developed an adaptive management process for the NPA and commenced its implementation in 2019. This management process is a combination of two encouraged catch levels corresponding to strong and weak recruitment levels, and a monitoring survey procedure to assess the level of recruitment. When a strong recruitment is detected by the monitoring survey (i.e., when catch per unit effort and the frequency of fat type are above the threshold levels in a certain number of consecutive survey tows), the higher encouraged catch level is applied in that fishing season. At the same time, specific areas in the southern ES region (where half of the catch occurred in the two recent years of strong recruitment, 2010 and 2012) are closed during the rest of fishing season, to conserve the spawning stock. When strong recruitment is not detected, the lower encouraged catch level is applied in that season. Although the management procedure is designed to balance the conservation of spawners with efficient utilization under both strong and weak recruitment levels, a careful evaluation of its effectiveness should be conducted, given the unpredictable fluctuation and lack of knowledge of the dynamics of this stock.

9. Marine Mammals

9.1. Cetaceans

(T. Tamura and Y. Kanaji)

In the western North Pacific subarctic region (SAR), at least 25 cetacean species (seven baleen and 18 toothed whales) have been recognized. In this region, some dedicated sighting surveys were conducted by the Institute of Cetacean Research (ICR) and the National Research Institute of Far Seas Fisheries (NRIFSF) of the Japan Fisheries and Education Agency. The second phase of the Japanese Whale Research Program under Special Permit in the North Pacific (JARPN), JARPN II, started with two feasibility surveys in 2000 and 2001. The full survey was conducted between 2002 and 2016. The research area of JARPN II was east of the Japanese coast, west of 170°E, north of 35°N, and south of the Russian and US Exclusive Economic Zone (Figure R23-13).

Based on 2008–2012 JARPN II, the number of several baleen whale species were estimated. Given that the area is a migration corridor of the whales, the numbers were estimated for the early season (May–June) and the late season (July–September). The estimates are summarized in Table R23-1 (Hakamada et al., 2016a, 2016b).

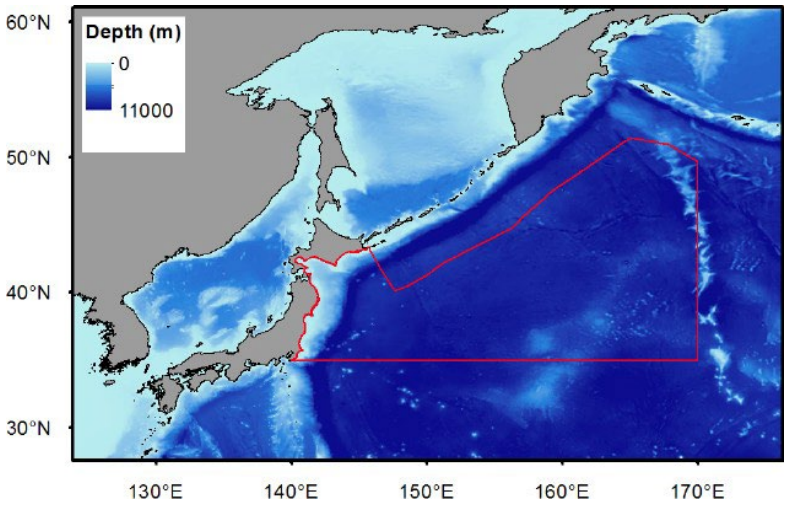

Figure R23-13. The survey area of the second phase of the Japanese Whale Research Program under Special Permit in the North Pacific (JARPN II) (red line). Bathymetry (m) is also shown.

Table R23-1. Abundance estimate for the common minke, sei, Bryde's, and sperm whales in the JARPN II survey area in early (2009 and 2011 + first survey in 2012 combined) and late season (2008). It is assumed that g(0) = 0.798 (CV = 0.134) for the common minke whale and g(0) = 1 for sei, Bryde's, and sperm whales.

Season/Year	Common minke		Sei		Bryde's		Sperm	
	P	CV (P)	**P**	CV (P)	**P**	CV (P)	**P**	CV (P)
Early								
2009	**3,629**	0.586	**4,734**	0.177	**2,957**	0.394	**11,459**	0.332
2011 + 2012	**2,122**	0.371	**2,988**	0.304	**1,851**	0.413	**11,652**	0.266
Late								
2008	**3,080**	0.677	**5,086**	0.378	**13,306**	0.251	**10,843**	0.358

Based on 2002–2013 JARPN II, seasonal spatial distributions of common minke, sei and Bryde's whales in the survey area were estimated by using generalized additive models (GAM). (Murase et al., 2016; Figure R23-14). All species shifted their distribution area toward the north of the survey area as the season progressed but the extents were different among species. Relative abundance of common minke whales was high in the coastal area of Japan. Relative abundance of sei whales was high in the offshore area of the survey area where SST was moderate within the area. Relative abundance of Bryde's whales was high in the southern part of the survey area where SST was high. The results suggest that spatial distributions of three baleen whale species were segregated in the JARPN II survey area although some overlaps occurred. The extent of direct competition (e.g., competitive exclusion of feeding area) could be minimal among the species but indirect competition for prey might occur, as they share the same prey species.

Stomach contents from sei, Bryde's and common minke whales sampled by 2000–2015 JARPN II showed that the three species are highly dependent on small pelagic fish, in addition to planktonic crustaceans. The change of prey compositions in sei whales among years drastically changed from Japanese anchovy in the early 2000s to Japanese sardine in 2014 and 2015, while the occurrence of *Neocalanus* copepods steadily continued throughout the years (Figure R23-15). The decrease in Japanese anchovy abundance synchronized with the catch record of Pacific stocks in Japanese fisheries. These results, suggesting a decrease in the amount of Japanese anchovy transported to offshore waters, is an important factor to determine the composition of the three baleen whale species in the JARPN II survey area.

Based on 2000–2007 JARPN II, stomach contents from 740 common minke, 489 sei and 393 Bryde's whales were examined (Konishi et al., 2009, 2016). The total seasonal prey consumption by the three baleen whale species in the survey area was estimated to be over 774 × 10^3 mt of Japanese anchovy, 140 × 10^3 mt of mackerel, and over 43 × 10^3 mt of Pacific saury, indicating these baleen whales are important components in the ecosystem, and warrant inclusion in fisheries assessments (Table R23-2). For small cetaceans, Kanaji et al. (2017) estimated the average abundance over 20 years for 14 species of Delphinidae and Phocoenidae using long-term sighting data from NRIFSF surveys conducted in summer from 1983–2006 (Figure R23-16). Total abundance estimates are summarized in Table R23-3. These estimates were obtained by spatial modelling with line-transect sampling.

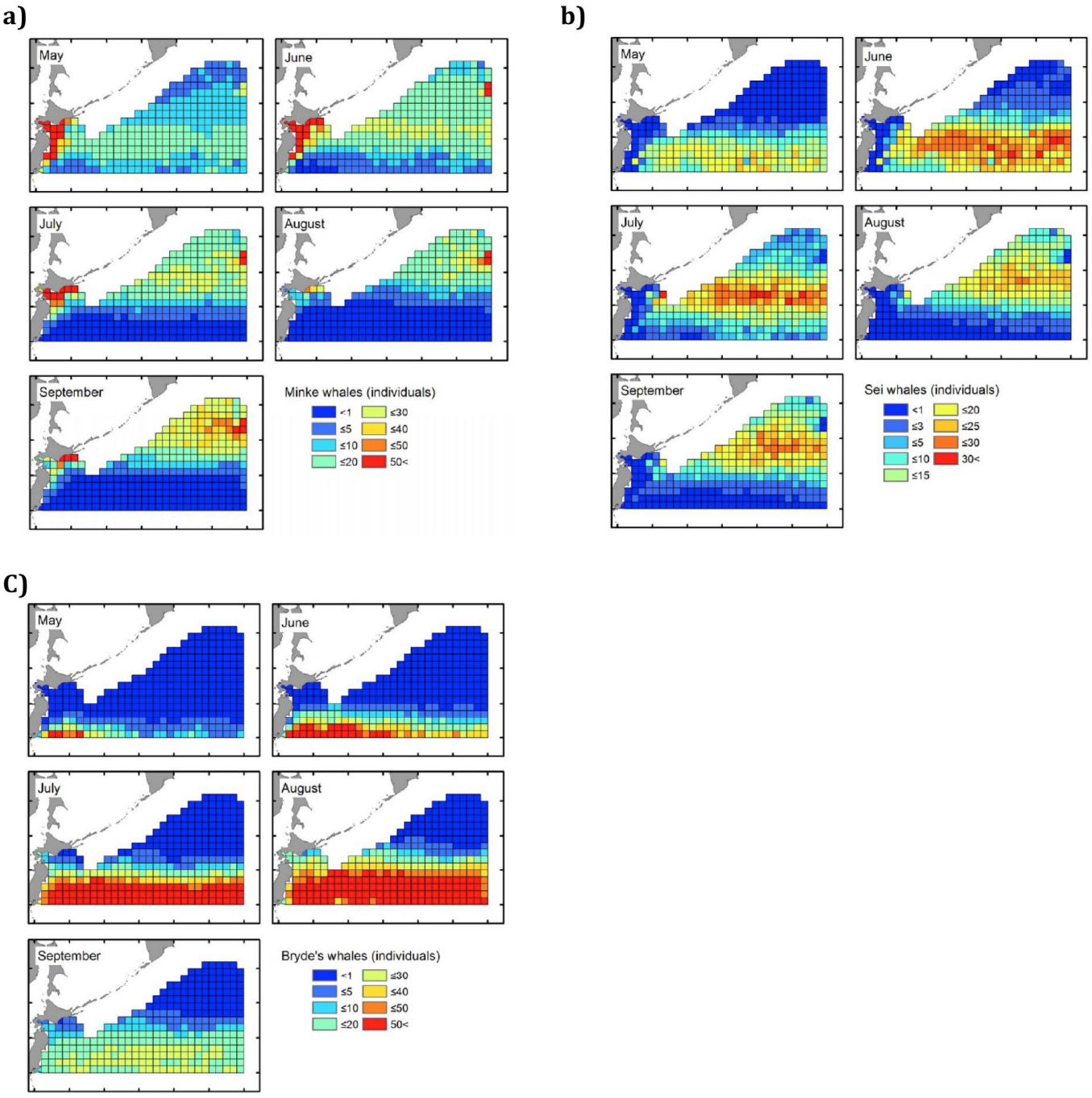

Figure R23-14. Estimated spatial distribution of (a) common minke, (b) sei and (c) Bryde's whales from May to September. Means of the estimated number of individuals in 1 × 1 longitude and latitude grids from 2002 to 2013 are shown.

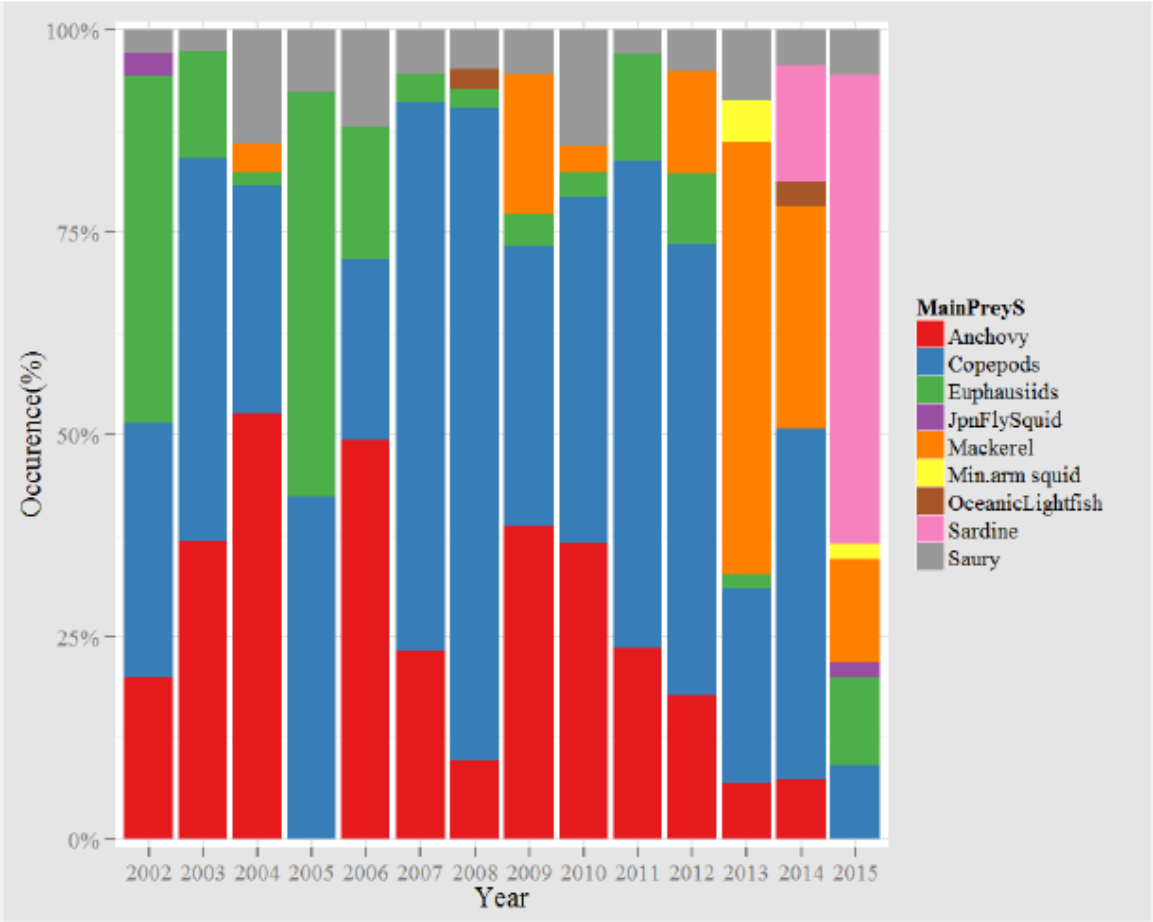

Figure R23-15. Trend of prey composition in the stomach contents of sei whales during 2002–2015 JARPN II.

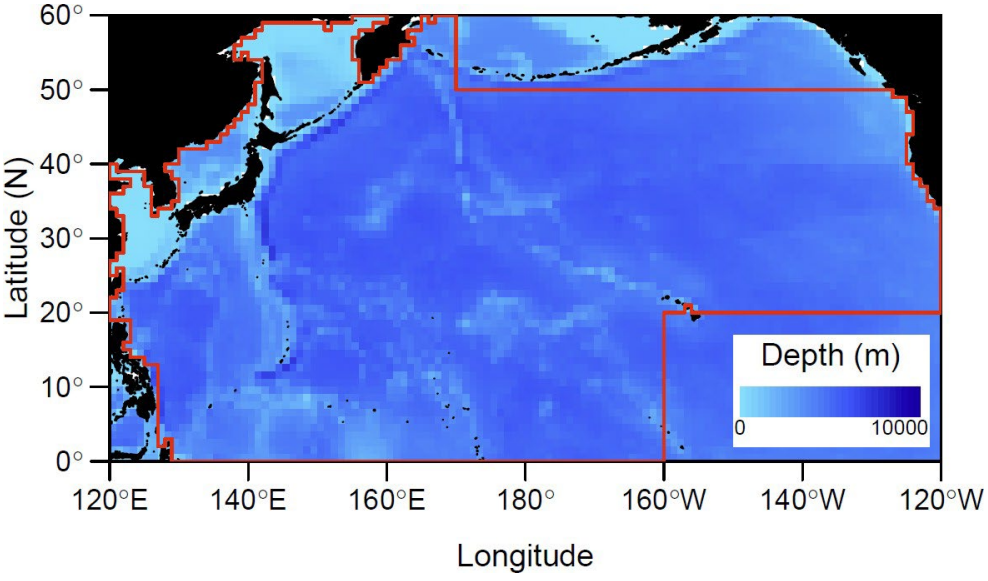

Figure R23-16. The area of National Research Institute of Far Seas Fisheries (NRIFSF) surveys (indicated by red lines) on average abundance of Delphinidae and Phocoenidae conducted in summer from 1983–2006. Modified from Kanaji et al. (2017).

Table R23-2. Estimated total prey consumption by three baleen whale species in the JARPNII study area, for the main prey species.

	Prey consumption (t)			
Prey species	Minke	Sei	Bryde's	Total
Japanese anchovy	75 925	278 638	419 852	774 415
Mackerels	8 237	118 432	13 813	140 023
Pacific saury	28 677	15 261	0	43 481

Table R23-3. Total abundance estimates over 20 years for 14 species of Delphinidae and Phocenidae in National Research Institute of Far Seas Fisheries (NRIFSF) survey areas (Figure R23-16) from 1983–2006.

Species name	Abundance	Coefficient of Variation
Spinner dolphin	904,473	0.20
Melon-headed whale	147,597	0.34
Rough-toothed dolphin	102,893	0.24
False killer whale	74,101	0.31
Pantropical spotted dolphin	1,886,022	0.20
Short-finned pilot whale	154,595	0.20
Common bottlenose dolphin	93,170	0.55
Risso's dolphin	349,309	0.24
Striped dolphin	1,766,025	0.15
Short-beaked common dolphin	1,428,857	0.42
Pacific white-sided dolphin	418,090	0.45
Northern right whale dolphin	56,899	0.52
Dall's porpoise	1,022,987	0.04
Killer whale	19,521	0.21

10. Pollutants/Contaminants

10.1. Anthropogenic radionuclides

(H. Kaeriyama)

Anthropogenic radionuclides in the ocean have been studied to determine their effect in marine ecology, and are used as a tracer to understand water movements and matter cycling. In March 2011, anthropogenic radionuclides were released into the ocean from the Fukushima Dai-ichi Nuclear Power Plant sites (Buesseler et al., 2011; Chino et al., 2011). The evaluation of radioactive cesium (^{134}Cs and ^{137}Cs) in the marine environment is important for addressing risks to both marine ecosystems and public health through consumption of fisheries products, because of their long half-life (2.07 years for ^{134}Cs and 30.07 years for ^{137}Cs). Prior to the Fukushima Dai-ichi Nuclear Power Plant accident, radioactive Cs entered the ocean via global fallout as a result of nuclear weapons testing held during the 1950s and 1980s (Bowen et al., 1980; Aarkrog, 2003). In the 2000s, ^{137}Cs concentration in the surface water was horizontally homogeneous and at a level of 1.5–2.0 Bq m^{-3} (Hirose and Aoyama, 2003; Povinec et al., 2004).

The total amount of ^{137}Cs released into the ocean by the Fukushima Dai-ichi Nuclear Power Plant accident was estimated to be 3–4 PBq (PBq = 10^{15} Bq) as direct release and 12–15 PBq as atmospheric deposition (cf. Aoyama et al., 2016). The activity ratios of ^{134}Cs/^{137}Cs, decay corrected to March–April 2011, were reported to be almost 1.0 for the entire North Pacific (e.g., Buesseler et al., 2011; Kaeriyama et al., 2014). This ratio means an equivalent amount of ^{134}Cs and ^{137}Cs was released into the ocean.

The Fukushima-derived radiocesium (^{134}Cs and ^{137}Cs) was able to spread broadly in the surface water, especially north of the Kuroshio Extension because the nuclear power plant is located at 37°25′N, 141°02′E, north of the Kuroshio Extension (Figure R23-17; Aoyama et al., 2013; Kaeriyama et al., 2013; Kumamoto et al., 2015). The surface dispersion of the Fukushima-derived ^{137}Cs can be described as three phases. First, atmospheric deposition resulted in a very patchy distribution over a broad area of the North Pacific and was immediately diluted; in the second phase, the directly released plume of Fukushima-derived radioactive Cs (> 10 Bq m^{-3} of ^{137}Cs) travelled eastward at mid-latitude; third, with the weakening of Kuroshio Extension flow with eastward dispersion in the central part of the North Pacific, the north–south dispersion of ^{137}Cs was enhanced and its concentration decreased markedly. Until December 2012, the main body of this Fukushima-derived radioactive Cs was located in the central part of the North Pacific (Kumamoto et al., 2015). For more details in the oceanic dispersion of Fukushima-derived radioactive Cs, see Kaeriyama (2017) and reference therein.

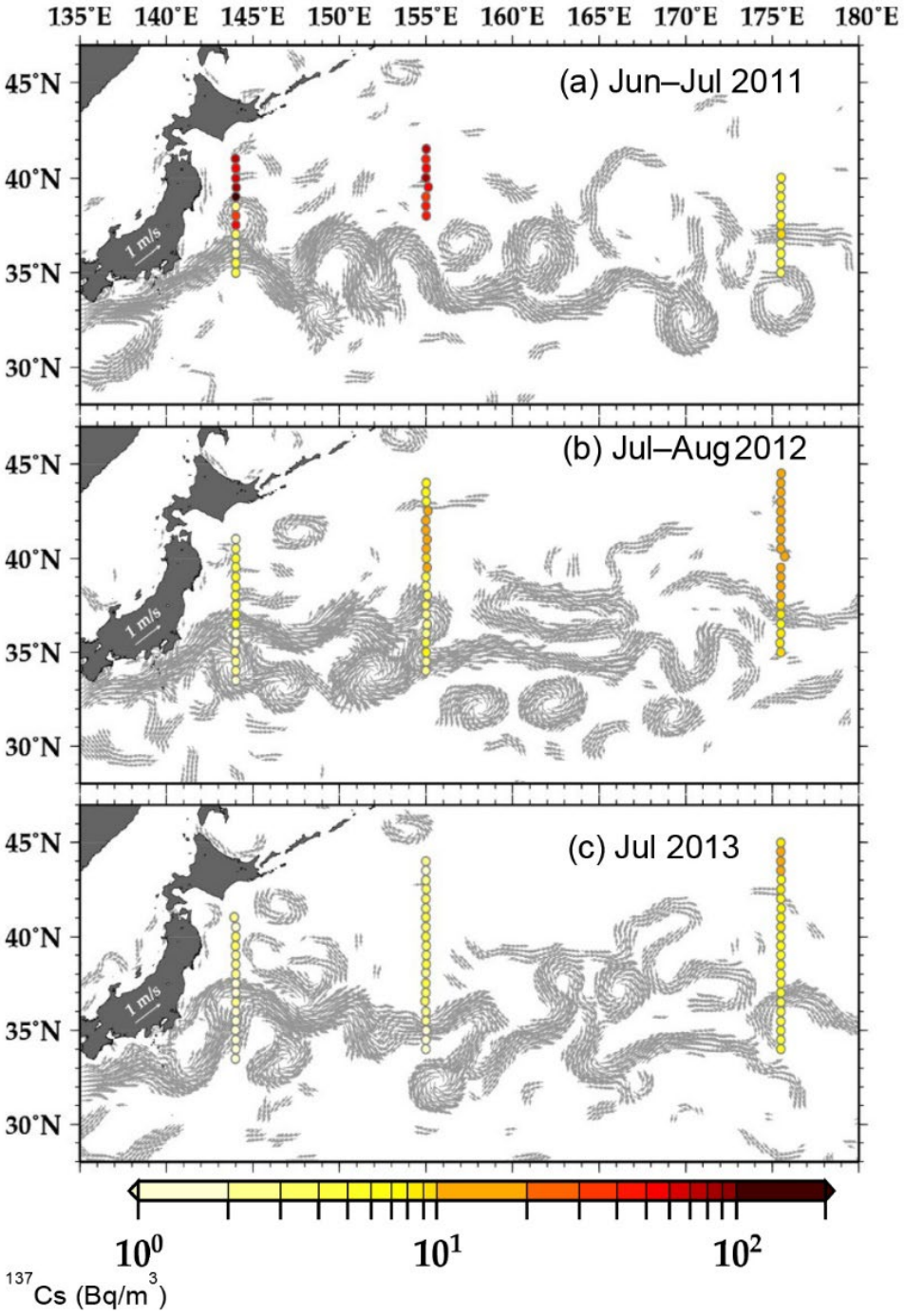

Figure R23-17. Concentration of ^{137}Cs in the surface seawater in the western and central North Pacific during (a) June 30 and July 29, 2011, (b) July 2 and 1 August, 2012, and (c) July 2–31, 2013. Color of the closed circles indicates concentration of ^{137}Cs. Gray arrows indicate estimated temporal mean velocity vectors for each sampling duration. Modified from Kaeriyama (2015).

10.2 Other contaminants

(S. Saito and N. Nagai)

The Japan Meteorological Agency (JMA) monitors heavy metals (cadmium and mercury) and floating pollutants (tar balls, floating plastics and petroleum hydrocarbons) in the western subarctic gyre (WSAG) region of the North Pacific (JMA, 2017). Here, the results of cadmium (Cd), floating tar balls, floating plastics and petroleum hydrocarbons are shown.

Time series of Cd concentration in surface water in the WSAG region (40°N–50°N, 140°E–165°E) from 1977 to 2015 are shown in Figure R23-18. Cd concentrations showed seasonal variations: high in winter and low in summer and autumn. These variations were attributed to Cd supply through entrainment and to removal by active biological consumption, but not to anthropogenic contamination (see Oyashio Section 4.4 in McKinnell and Dagg, 2010). Although the annual mean concentration of Cd before 1989 was high (60 ± 39 ng kg^{-1}), it significantly decreased to 38 ± 21 ng kg^{-1} after 1991.

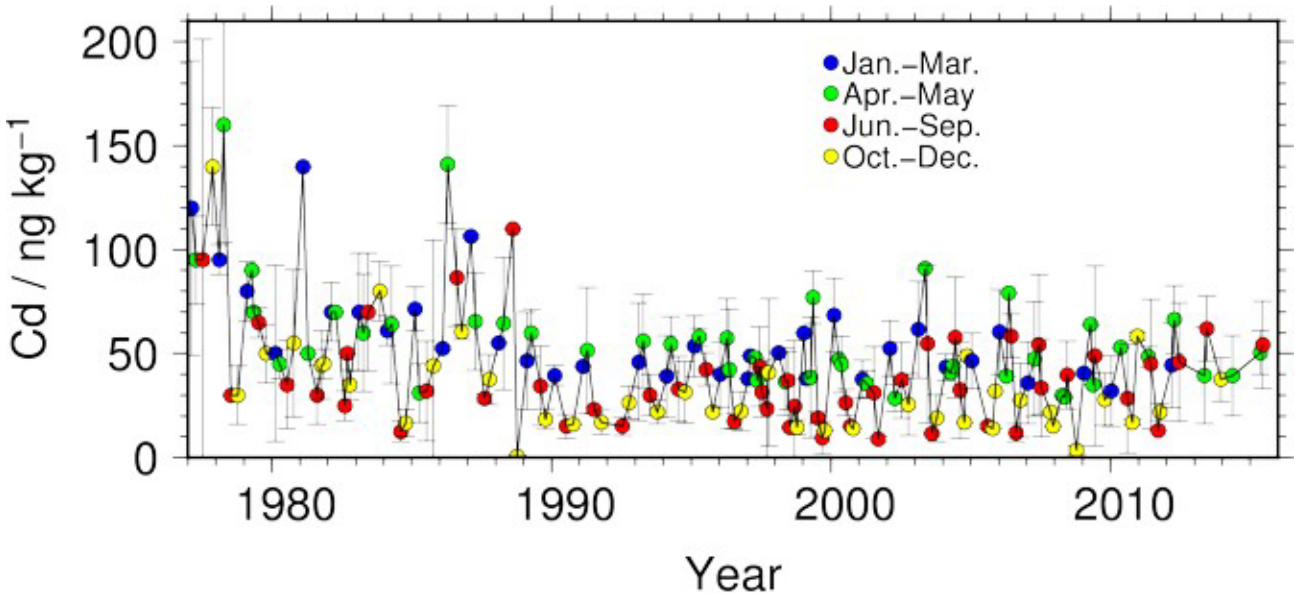

Figure R23-18. Temporal variation of cadmium (Cd) concentrations in surface water in the region of 40°N–50°N, 140°E–165°E for 1977–2015. The mean in each month is plotted. Solid colored circles indicate the season. Error bars indicate the standard deviation for each month.

Floating tar balls were observed with a horizontal towing net of 0.35 mm mesh at the region of 35°N–50°N, 140°E–165°E. Time series of tar ball concentrations is shown in Figure R23-19. In this region, 0 to 24 (average, 12) samples per a year were obtained during the period of 1977–2015. Before 1983, the concentration of tar balls was high (average, 0.12 mg m^{-2}). High tar ball concentrations exceeding 0.1 mg m^{-2} were found until 1993. After 2000, the tar ball concentrations were low (average, 0.004 mg m^{-2}) and few tar balls were collected, although a high tar ball concentration was occasionally observed in 2004 (0.23 mg m^{-2}).

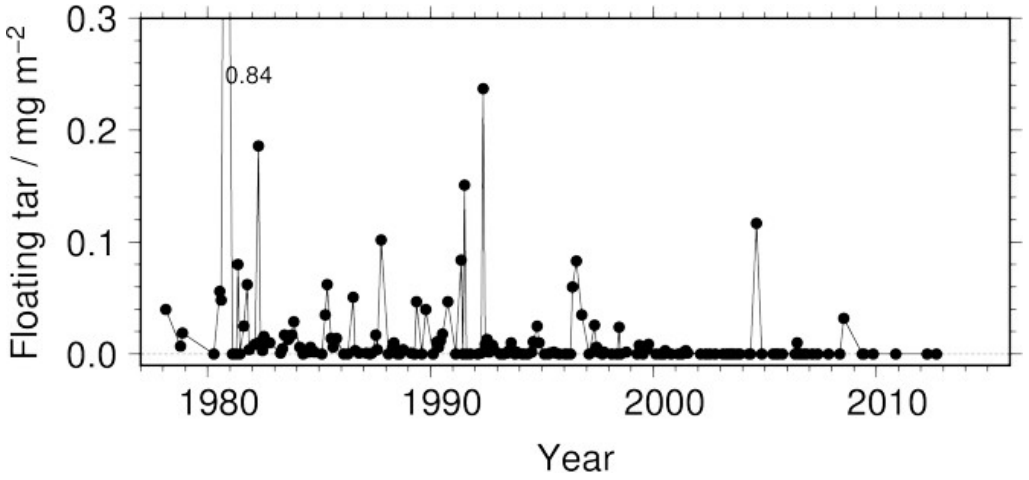

Figure R23-19. Temporal variation of floating tar balls collected in the region of 40°N–50°N, 140°E–165°E for 1978–2012. Each plot indicates the monthly mean.

Floating plastics (e.g.,plastic bottles or drifting floats) were visually counted during the cruising period from 1978 to 2015, and the number was calculated for every 100 km of cruise distance. The average for each month in the region of 40°N–50°N, 140°E–165°E is shown in Figure R23-20. A large number of floating plastics were observed in 1985–1995 (average of 16 pieces per 100 km for the entire period). The plastics decreased in 2000–2010 (average of 5 pieces per 100 km), occasionally exceeding 20 pieces per 100 km. Floating plastics released to the open ocean by the Great East Japan Earthquake and tsunami on March 11, 2011 have also been observed.

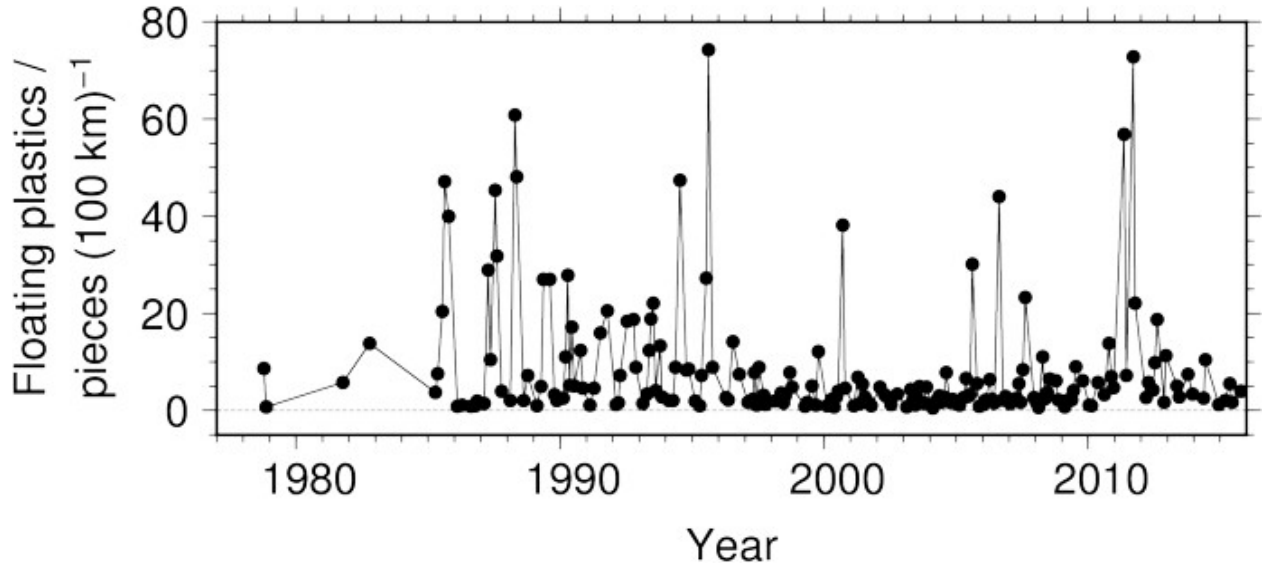

Figure R23-20. Temporal variation of floating plastics in the region of 40°N–50°N, 140°E–165°E for 1978–2015. Each plot indicates the monthly mean. These plastics were observed visually from the bridge of the ship.

The concentrations of petroleum hydrocarbons in surface water in the region of 40°N–50°N, 140°E–165°E were high (average 227 ng kg^{-1}) before 1991 (Figure R23-21). After 2002, the hydrocarbon concentrations were low (averages, 33 ng kg^{-1}) compared with levels in 1995–2002 (average 73 ng kg^{-1}).

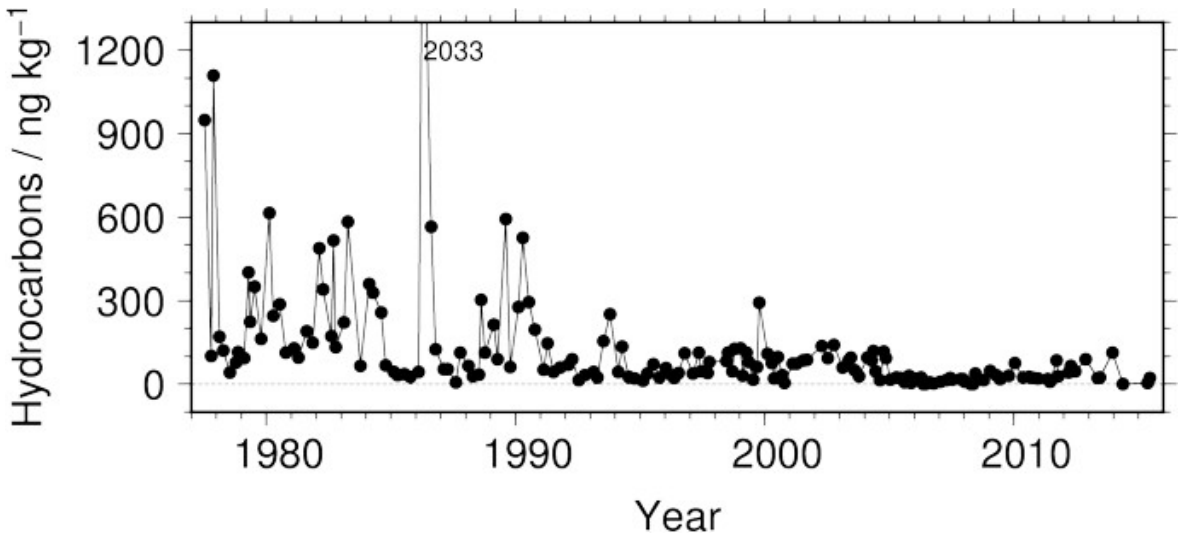

Figure R23-21. Temporal variation of petroleum hydrocarbon concentration in surface water in the region of 40°N–50°N, 140°E–165°E for 1977–2015. Each plot indicates the monthly mean.

11. Climate Change, Ecosystem Considerations and Emerging Issues

A northward shrinking of the WSAG was detected after 1990 (section 4, Figure R23-2, and this process caused an increase of the MLD in the WSAG north of 47°N while it shoaled south of 47°N (section 6, Figure R23-7c). Other changes in physical–chemical conditions of the WSAG after 1990 were PDO-related ones, such as an increase in SST (section 6, Figure R23-7b) and decrease of MLD nutrients (Section 5.1, Figure R23-3. Note that the PDO was in a decreasing phase after the 1990s, and hence a positive relationship between the PDO and MLD nutrients indicates that nutrient concentrations decreased after 1990.) Chl-*a* concentrations in the WSAG increased in the area north of 47°N after the 1990s (Section 6, Figure R23-7), and this is interpreted to be a result of phytoplankton being more sensitive to an increase in SST than to reduced nutrients (Figure R23-7) and low-light conditions arising from an increase in the MLD. Decreasing Chl-*a* concentrations south of 47°N are easier to understand, as lower-trophic biomass is generally sensitive to nutrient decrease in the subtropical-subarctic transition area (e.g., Tadokoro et al., 2009). Zooplankton biomass did not show significant trends after 1990, but a northward shift of warm-water copepods (Section 6, Figure R23-9c) seems to correspond to the northward shift of the WSAG during this period. In summary, the lower-trophic ecosystem in the WSAG revealed variations conforming to changes in physical–chemical conditions in this area.

Pelagic fishes have recently shown significant changes related to a regime shift (see Chapter R18), and the prey composition of sei whales seem to reflect such a change of the pelagic fish composition. As each regional report of NPESR-3 mainly treats recent changes of the ocean environment and ocean ecosystem, we will need to have additional schemes to discuss multi-decadal issues such as regime-shift events.

Several monitoring results for ocean contaminants, including anthropogenic radionuclides, suggest that the WSAG area is healthy, but ocean acidification is still continuing (Section 5.2) and we must continue watching its impact on the ocean ecosystem. Ocean deoxygenation is intensively discussed in Chapter R18 (Oyashio) and data observed in the WSAG are also included there, so we omit this issue in this chapter. However, we would like to mention that ocean deoxygenation is also ongoing in the subsurface area of the WSAG, simultaneously with ocean acidification.

References

Aarkrog, A. 2003. Input of anthropogenic radionuclides into the World Ocean. Deep-Sea Res. II 50: 2597–2606, https://doi.org/10.1016/S0967-0645(03)00137-1

Aoyama, M., Tsumune, D., and Hamajima, Y. 2013. Distribution of ^{137}Cs and ^{134}Cs in the North Pacific Ocean: Impacts of the TEPCO Fukushima-Daiichi NPP accident. J. Radioanal. Chem. 296: 535–539, https://doi.org/10.1007/s10967-012-2033-2

Aoyama, M., Hamajima, Y., Hult, M., Uematsu, M., Oka, E., Tsumune, D., and Kumamoto, Y. 2016. 134Cs and 137Cs in the North Pacific Ocean derived from the TEPCO Fukushima Dai-ichi Nuclear Power Plant accident, Japan in March 2011: Part One – Surface pathway and vertical distributions. J. Oceanogr. 72: 53–65, https://doi.org/10.1007/s10872-015-0335-Z

Bates, N.R., Astor, Y.M., Church, M.J., Currie, K., Dore, J.E., González-Dávila, M., Lorenzoni, L., Muller-Karger, F., Olafsson, J., and Santana-Casiano, J.M. 2014. A time-series view of changing ocean chemistry due to ocean uptake of anthropogenic CO_2 and ocean acidification. Oceanography 27: 126–141, https://doi.org/10.5670/oceanog.2014.16

Batten, S.D., Welch, D.W., and Jonas, T. 2003. Latitudinal differences in the duration of development of *Neocalanus plumchrus* copedodites. Fish. Oceanogr. 12: 201–208, https://doi.org/10.1046/j.1365-2419.2003.00233.x

Boehlert, G.W. and Sasaki, T. 1988. Pelagic biogeography of the armorhead, *Pseudopentaceros wheeleri*, and recruitment to isolated seamounts in the North Pacific Ocean. Fish. Bull. 86: 453–466.

Bornhold, E., Mackas, D., and Harrison, P. 1998. Interdecadal variations in developmental timing of the copepod *Neocalanus plumchrus* (Marukawa) in the Strait of Georgia. Eos 79: 102 (Abstract).

Bowen, V.T., Noshkin, V.E., Livingston, H.D., and Volchok, H.K. 1980. Fallout radionuclides in the Pacific Ocean: Vertical and horizontal distributions, largely from GEOSECS stations. Earth Planet. Sci. Lett. 49: 411–434.

Buesseler, K.O., Aoyama, M., and Fukasawa, M. 2011. Impacts of the Fukushima Nuclear Power Plants on marine radioactivity. Environ. Sci. Tech. 45: 9931–9935, https://doi.org/10.1021/es202816c

Byrne, R.H., Mecking, S., Feely, R.A., and Liu, X. 2010. Direct observations of basin-wide acidification of the North Pacific Ocean. Geophys. Res. Lett. 37: L02601, https://doi.org/10.1029/2009GL040999

Chihara, M. and Murano, M. 1997. An Illustrated Guide to Marine Plankton in Japan. Tokai University Press, Tokyo, 1574 pp. (in Japanese)

Chino, M., Nakayama, H., Nagai, H., Terada, H., Katata, G., and Yamazawa, H. 2011. Preliminary estimation of release amounts of ^{131}I and ^{137}Cs accidentally discharged from the Fukushima Daiichi Nuclear Power Plant into the atmosphere. J. Nucl. Sci. Tech. 48: 1129–1134, https://doi.org/10.1080/18811248.2011.9711799

Dlugokency, E.J., Masarie, K.A., Lang, P.M., and Tans, P.P. 2014. NOAA Greenhouse Gas Reference from Atmospheric Carbon Dioxide Dry Air Mole Fractions from the NOAA ESRL Carbon Cycle Cooperative Global Air Sampling Network, Data Path: ftp://aftp.cmdl.noaa.gov/data/trace_gases/co2/flask/surface/

Dodimead, A.J., Favorite, F., and Hirano, T. 1963. Winter oceanographic conditions in the central Subarctic Pacific. Bull. Int. N. Pac. Comm. 13: 1–195.

Doney, S.C., Fabry, V.J., Feely, R.A., and Kleypas, J.A. 2009. Ocean acidification: The other CO_2 problem. Ann. Rev. Mar. Sci. 1: 169–192, https://doi.org/10.1146/annurev.marine.010908.163834

Dore, J.E., Lukas, R., Sadler, D.W. Church, M.J., and Karl, D.M. 2009. Physical and biogeochemical modulation of ocean acidification in the central North Pacific. Proc. Nat. Acad. Sci. USA 106: 12,235–12,240, https://doi.org/10.1073/pnas.0906044106

FAO (Food and Agriculture Organization) 2016. The State of World Fisheries and Aquaculture, Food and Agriculture Organization of the United Nations, Rome, http://www.fao.org/3/a-i5555e.pdf

Favorite F., Dodimead, A.J., and Nasu, K. 1976. Oceanography of the subarctic Pacific region. Bull. Int. N. Pac. Comm. 33: 1–187.

Feely, R.A., Sabine, C.L., Lee, K., Berelson, W., Kleypas, J., Fabry, V.J., and Millero, F. J. 2004. Impact of anthropogenic CO_2 on the $CaCO_3$ system in the oceans. Science 305: 362–366, https://doi.org/10.1126/science.109732926

Fujiki, T., Matsumoto, K., Mino, Y., Sasaoka, K., Wakita, M., Kawakami, H., Honda, M.C., Watanabe, S., and Saino, T. 2014. Seasonal cycle of phytoplankton community structure and photophysiological state in the western subarctic gyre of the North Pacific. Limnol. Oceanogr. 59: 887–900, https://doi.org/10.4319/lo.2014.59.3.0887

Hakamada, T. and Matsuoka, K. 2016a. The number of western North Pacific common minke, Bryde's and sei whales distributed in JARPNII offshore survey area. Paper SC/F16/JR12 presented to the JARPNII special permit expert panel review workshop, Tokyo, February 2016 (unpublished), 13 pp.

Hakamada, T. and Matsuoka, K. 2016b. The number of sperm whales in the western North Pacific in the JARPN II offshore survey area. Paper SC/F16/JR14 presented to the JARPNII special permit expert panel review workshop, Tokyo, February 2016 (unpublished), 8 pp.

Hirose, K. and Aoyama, M. 2003. Present background levels of surface ^{137}Cs and $^{239,240}Pu$ concentrations in the Pacific. J. Environ. Radioact. 69: 53–60, https://doi.org/10.1016/S0265-931X(03)00086-9

IPCC (Intergovernmental Panel on Climate Change) 2013. The Physical Science Basis. Contribution of Working Group I to the Fifth Assessment Report of the Intergovernmental Panel on Climate Change, edited by T.F. Stocker et al., Cambridge Univ. Press, Cambridge, U.K.

JMA (Japan Meteorological Agency). 2017. Annual Report on Atmospheric and Marine Environment Monitoring Data, http://www.data.jma.go.jp/gmd/env/data/report/data/index_e.html

Kaeriyama, H., Ambe, D., Shimizu, Y., Fujimoto, K., Ono, T., Yonezaki, S., Kato, Y., Matsunaga, H., Minami, H., Nakatsuka, S., and Watanabe, T. 2013. Direct observation of ^{134}Cs and ^{137}Cs in surface seawater in the western and central North Pacific after the Fukushima Dai-ichi nuclear power plant accident. Biogeosciences 10: 4287–4295, https://doi.org/10.5194/bg-10-4287-2013

Kaeriyama, H., Shimizu, Y., Ambe, D., Masujima, M., Shigenobu, Y., Fujimoto, K., Ono, T., Nishiuchi, K., Taneda, T., Kurogi, H., Setou, T., Sugisaki, H., Ichikawa, T., Hidaka, K., Hiroe, Y., Kusaka, A., Kodama, T., Kuriyama, M., Morita, H., Nakata, K., Morinaga, K., Morita, T., and Watanabe, T. 2014. Southwest intrusion of ^{134}Cs and ^{137}Cs derived from the Fukushima Dai-ichi Nuclear Power Plant accident in the western North Pacific. Environ. Sci. Tech. 45: 3120–3127, https://doi.org/10.1021/es403686

Kaeriyama, H. 2015. Chapter 2. ^{134}Cs and ^{137}Cs in the seawater around Japan and in the North Pacific. In: Impacts of the Fukushima Nuclear Accident on Fish and Fishing Grounds. Nakata, K. and Sugisaki, H. (eds.), Springer, Japan, pp. 11–32.

Kaeriyama, H. 2017. Oceanic dispersion of Fukushima-derived radioactive cesium: a review. Fish. Oceanogr. 26: 99–113, doi:10.1111/fog.12177

Kanaji, Y., Okazaki, M., and Miyashita, T. 2017. Spatial patterns of distribution, abundance, and species diversity of small odontocetes estimated using density surface modeling with line transect sampling. Deep-Sea Res. II. 140: 151–162, https://doi.org/10.1016/j.dsr2.2016.05.014

Kiyota, M., Nishida, K., Murakami, C., and Yonezaki, S. 2016. History, biology, and conservation of Pacific endemics. 2. The North Pacific armorhead, *Pentaceros wheeleri* (Hardy, 1983) (Perciformes, Pentacerotidae). Pac. Sci. 70: 1–20, https://doi.org/10.2984/70.1.1

Kobari, T. and Ikeda, T. 2001. Ontogenetic vertical migration and life cycle of *Neocalanus plumchrus* (Crustacea: Copedoda) in the Oyashio region, with notes on regional variations in body sizes. J. Plankt. Res. 23: 287–302, https://doi.org/10.1093/plankt/23.3.287

Kobari, T., Tadokoro, K., Sugisaki, H., and Itoh. H. 2007. Response of *Eucalanus bungii* to oceanographic conditions in the western subarctic Pacific Ocean: retrospective analysis of the Odate Collections. Deep-Sea Res. II 54: 23–26, https://doi.org/10.1016/j.dsr2.2007.08.005

Konishi, K., Tamura, T., Isoda, T., Okamoto, R., Hakamada, T., Kiwada, H., and Matsuoka, K. 2009. Feeding strategies and prey consumption of three baleen whale species within the Kuroshio-Current Extension. J. Northw. Atl. Fish. Sci. 42: 27–40, https://doi.org/10.2960/J.v42.m648

Konishi, K., Isoda, T., and Tamura, T. 2016. Decadal change of feeding ecology in sei, Bryde's and common minke whales in the offshore of the Western North Pacific. Paper SC/F16/JR23 presented to the JARPNII special permit expert panel review workshop, Tokyo, February 2016 (unpublished), 19 pp.

Kumamoto, Y., Aoyama, M., Hamajima, Y., Nishino, S., Murata, A., and Kikuchi, T. 2015. Meridional distribution of Fukushima-derived radiocesium in surface seawater along a trans-Pacific line from the Arctic to Antarctic Oceans in summer 2012. J. Radioanal. Nucl. Chem. 307: 1703–1710, https://doi.org/10.1007/s10967-015-4439-0

Matsumoto, K., Honda, M.C., Sasaoka, K., Wakita, M., Kawakami, H., and Watanabe, S. 2014. Seasonal variability of primary production and phytoplankton biomass in the western Pacific subarctic gyre: Control by light availability within the mixed layer. J. Geophys. Res. 119: 6523–6534, https://doi.org/10.1002/2014JC009982

McKinnell, S.M. and Dagg, M.J. (Eds.) 2010. Marine Ecosystems of the North Pacific Ocean, 2003-2008. PICES Spec. Pub. 4, 393 pp.

Moon, D.-Y. 2017. Birth of the North Pacific Fisheries Commission (NPFC). Ocean Newslett. 400: 13–14.

Murakami, C., Yonezaki, S., Suyama, S., Nakagami, M., Okuda, T., and Kiyota, M. 2016. Early pelagic life-history characteristics of North Pacific armorhead *Pentaceros wheeleri*. Fish. Sci. 82: 709–718, https://doi.org/10.1007/s12562-016-1002-z

Murase, H., Hakamada, T., Sasaki, H., Matsuoka, K., and Kitakado, T. 2016. Seasonal spatial distributions of common minke, sei and Bryde's whales in the JARPNII survey area from 2002 to 2013. Paper SC/F16/JR7 presented to the JARPNII special permit expert panel review workshop, Tokyo, February 2016 (unpublished), 17 pp.

Nagano, A., Wakita, M., and Watanabe, S. 2016. Dichothermal layer deepening in relation with halocline depth change associated with northward shrinkage of North Pacific western subarctic gyre in early 2000s. Ocean Dynam. 66: 163–172, https://doi.org/10.1007/s10236-015-0917-8

Nakaoka, S., Telszewski, M., Nojiri, Y., Yasunaka, S., Miyazaki, C., Mukai, H., and Usui, N. 2013. Estimating temporal and spatial variation of sea surface pCO_2 in the North Pacific using a self-organizing map neural network technique. Biogeosciences 10: 6093–6106. https://doi.org/10.5194/bgd-10-4575-2013

Nathans, L.L., Oswald, F.L., and Nimon, K. 2012. Interpreting multiple linear regression: a guidebook of variable importance. Pract. Assess. Res. Eval. 17: https://doi.org/10.7275/5fex-b874

Nishida, K., Murakami, C., Yonezaki, S., Miyamoto, M., Okuda T., and Kiyota, M. 2016. Prey use by three deep-sea fishes in the Emperor Seamount waters, North Pacific Ocean, as revealed by stomach contents and stable isotope analyses. Environ. Biol. Fishes 99: 335–349, https://doi.org/10.1007/s10641-016-0477-x

Orr, J., Fabry, V.J, Aumont, O., Bopp, L., Doney, S.C., Feely, R.A., Gnanadesikan, A., Gruber, N., Ishida, A., Foos, F., Key, R.M., Lindsay, K., Maier-Reimer, E., Matear, R., Monfray, P., Mouchet, A., Najjar, R.G., Plattner, G.-K., Rodgers, K. B., Sabine, C.L., Sarmiento, J.L., Schlitzer, R., Slater, R.D., Totterdell, I.J., Weirig, M.-F., Yamanaka, Y., and Yool, A. 2005. Anthropogenic ocean acidification over the twenty-first century and its impact on calcifying organisms. Nature 437: 681–686, https://doi.org/10.1038/nature04095

Palevsky, H.I., Quay, P., Lockwood, D.E., and Nicholson, D. 2015. The annual cycle of gross primary production, net community production and export efficiency across the North Pacific Ocean. Global Biogeochem. Cycles 30: 361–380, https://doi.org/10.1002/2015GB005318

Povinec, P.P., Hirose, K., Honda, T., Ito, T., Marian Scot, E., and Togawa, O. 2004. Spatial distribution of ^{3}H, ^{90}Sr, ^{137}Cs and $^{239,240}Pu$ in surface waters of the Pacific and Indian Oceans- GLOMARD database. J. Environ. Radioact. 76: 113–137, https://doi.org/10.1016/j.jenvrad.2004.03.022

Saito, H., Tsuda, A., and Kasai, H. 2002. Nutrient and plankton dynamics in the Oyashio region of the western subarctic Pacific Ocean. Deep-Sea Res. II 49: 5463–5486, https://doi.org/10.1016/S0967-0645(02)00204-7

Siswanto, E., Honda, M.C., Matsumoto, K., Sasai, Y., Fujiki, T., Sasaoka, K., and Saino, T. 2016a. Sixteen-year phytoplankton biomass trends in the northwestern Pacific Ocean observed by the SeaWiFS and MODIS ocean color sensors. J. Oceanogr. 72: 479–489, https://doi.org/10.1007/s10872-016-0357-1

Siswanto, E., Honda, M.C., Sasai, Y., Sasaoka, and K., Saino, T. 2016b. Meridional and seasonal footprints of the Pacific Decadal Oscillation on phytoplankton biomass in the northwestern Pacific Ocean. J. Oceanogr. 72: 465–477, https://doi.org/10.1007/s10872-016-0367-z

Steinberg, D., Cope J.S., Wilson S.E., and Kobari, T. 2008. A comparison of mesopelagic mesozooplankton community structure in the subtropical and subarctic Pacific Ocean. Deep-Sea Res. II 55: 1615–1635, https://doi.org/10.1016/j.dsr2.2008.04.025

Tadokoro, K., Ono, T., Yasuda, I., Osafune, S., Shiomoto, A., and Sugisaki, H. 2009. Possible mechanisms of decadal-scale variation in PO_4 concentration in the western North Pacific. Geophys. Res. Lett. 36: L08606. https://doi.org/10.1029/2009GL037327

Takahashi, K. and Ide, K. 2011. Reproduction, grazing, and development of the large subarctic calanoid *Eucalanus bungii*: in the spring diatom bloom the key to controlling their recruitment? Hydrobiologia 666: 99–109, https://doi.org/10.1007/s10750-010-0093-2

Tsuda, A., Takeda, S., Saito, H., Nishioka, J., Nojiri, Y., Kudo, I., Kiyosawa, H., Shiomoto, A., Imai, K., Ono, T., Shimamoto, A., Tsumune, D., Yoshimura, T., Aono, T., Hinuma, A., Kinugasa, M., Suzuki, K., Sorin, Y., Noiri, Y., Tani, H., Deguchi, Y., Tsurushima, N., Ogawa, H., Fukami, K., Kuma, T., and Saino, T. 2003. A mesoscale iron enrichment in the western subarctic Pacific induces large centric diatom bloom. Science 300: 958–961, https://doi.org/10.1126/science.10820000

Tsuda, A., Saito, H., and Kasai, H. 2004. Life histories of *Eucalanus bungii* and *Neocalanus cristatus* (Copepoda: Calanoida) in the western subarctic Pacific Ocean. Fish. Oceanogr. 13: 10–20, https://doi.org/10.1111/j.1365-2419.2004.00315.x

Tsurushima, N., Nojiri, Y., Imai, K., and Watanabe, S. 2002. Seasonal variations of carbon dioxide system and nutrients in the surface mixed layer at Station KNOT (44°N, 155°E) in the subarctic North Pacific. Deep-Sea Res. II 49: 5377–5394, https://doi.org/10.1016/S0967-0645(02)00197-2

Wakita M., Watanabe, S., Murata, A., Tsurushima, N., and Honda, M. 2010. Decadal change of dissolved inorganic carbon in the subarctic western North Pacific Ocean. Tellus 62B: 608–620, https://doi.org/10.1111/j.1600-0889.2010.00476.x

Wakita M., Watanabe, S., Honda, M., Nagano, A., Kimoto, K., Matsumoto, K., Kitamura, M., Sasaki, K., Kawakami, H., Fujiki, T., Sasaoka, K., Nakano, Y., and Murata, A. 2013. Ocean acidification from 1997 to 2011 in the subarctic western North Pacific Ocean. Biogeosciences 10: 7817–7827, https://doi.org/10.5194/bg-10-7817-2013

Wakita, M. Honda, M.C., Matsumoto, K., Fujiki, T., Kawakami, H., Yasunaka, S., Sasai, Y., Sukigara, C., Uchimiya, M., Kitamura, M., Kobari, T., Mino, Y., Nagano, A., Watanabe, S., and Saino, T. 2016. Biological organic carbon export estimated from the annual carbon budget observed in the surface waters of the western subarctic and subtropical North Pacific Ocean from 2004 to 2013. J. Oceanogr. 72: 665–685, https://doi.org/10.1007/s10872-016-0379-8

Wakita M., Nagano, A., Fujiki, T., and Watanabe, S. 2017. Slow acidification of the winter mixed layer in the subarctic western North Pacific. J. Geophys. Res. 122: 6923–6935, https://doi.org/10.1002/2017JC013002

Weiss, R. and Price, B.A. 1980. Nitrous oxide solubility in water and seawater. Mar. Chem. 8: 347–359, https://doi.org/10.1016/0304-4203(80)90024-9

Whitney, F.A. 2011. Nutrient variability in the mixed layer of the subarctic Pacific Ocean, 1987– 2010. J. Oceanogr. 67: 481–492, https://doi.org/10.1007/s10872-011-0051-2

Yasunaka, S., Nojiri, Y., Nakaoka, S., Ono, T., Mukai, H., and Usui, N. 2013. Monthly maps of sea surface dissolved inorganic carbon in the North Pacific: Basin-wide distribution and seasonal variation. J. Geophys. Res. 118: 3843–3850, https://doi.org/10.1002/jgrc.20279

Yasunaka, S., Nojiri, Y., Nakaoka, S.-I., Ono, T., Whitney, F., and Telszewski, M. 2014a. Mapping of sea surface nutrients in the North Pacific: Basin-wide distribution and seasonal to interannual variability. J. Geophys. Res. 19: 7756–7771, https://doi.org/10.1002/2014JC010318

Yasunaka, S., Nojiri, Y., Nakaoka, S., Ono, T., Mukai, H., and Usui, N. 2014b. North Pacific dissolved inorganic carbon variations related to the Pacific decadal oscillation. Geophys. Res. Lett. 41: 1005–1011, https://doi.org/10.1002/2013GL058987

Yasunaka, S., Ono, T., Nojiri, Y., Whitney, F.A., Wada, C., Murata, A., Nakaoka, S.-I., and Hosoda, S. 2016. Long-term variability of surface nutrient concentrations in the North Pacific. Geophys. Res. Lett. 43: 3389–3397, https://doi.org/10.1002/2016GL068097

Yoshiki, T., Chiba, S., Sasaoka, K., Ono, T., and Batten, S. 2013. Interannual and regional variations in abundance patterns and developmental timing in mesozooplankton of the western North Pacific Ocean based on Continuous Plankton Recorder during 2001–2009. J. Plankt. Res. 35: 993–1008, https://doi.org/10.1093/plankt/fbt047

Yoshiki, T., Chiba, S., Sasaki, Y., Sugisaki, H., Ichikawa, T., and Batten, S. 2015. Northerly shift of warm-water copepods in the western subarctic North Pacific: Continuous plankton recorder samples (2001-2013). Fish. Oceanogr. 24: 414–429, https://doi.org/10.1111/fog.12119